NTNU – Trondheim
Norwegian University of
Science and Technology

Calibration methodologies for multi-giga sample per second ADCs

Kai Erik Hoff

Electronics System Design and Innovation
Submission date: June 2014
Supervisor: Lars Magne Lundheim, IET

Norwegian University of Science and Technology
Department of Electronics and Telecommunications

Norwegian University of Science and Technology
Department of Electronics and Telecommunications

Master Thesis

Calibration Methodologies for Multi-Giga Sample per Second ADCs

Author:
Kai Erik Hoff

Supervisor:
Prof. Lars Lundheim

June 19, 2014

Abstract

Time-interleaving Analog-to-Digital Converters allows for increased sampling rates at the cost of added signal distortion. This article considers a system where Timing Jitter is counteracted by a Trace and Hold module, and investigates existing calibration methods for Offset and Gain mismatch which either make use of an additive calibration sequence, calculates and compares subchannel energy, or bandlimits the input signal. Certain modifications are made to each of the algorithms allowing more versatile systems, or higher performance.

The performance of a calibration method will be judged by it's average estimation error, possible worst-case outcomes and their impact on the system's stability. A number of modifications which aim to potentially reduce the Mean Square Error or improve the estimator's diversity are introduced. The various systems are tested using both white noise input, and inputs containing several sinusoidal components.

The numerical simulations illustrate some of the difficulties involved in designing a blind or partially blind Gain calibration system, compared to one relying on a training signal. For the method using a training signal, an algorithm designed to resemble a Maximum A Posteriori estimator is shown to offer increased performance. The modifications to the Gain calibration method are shown to be moderately beneficial, depending on the situation. The calibration system which relies on oversampling is modified so it can be expanded to calibrate Gain mismatch for any even number of ADCs, which is shown to work under certain circumstances.

Acknowledgements

The work on this thesis masters thesis has taken place during the spring of 2014 at the Norwegian University of Science and Technology. The work is based on a project in the same field conducted during the fall of 2013. The objective of this thesis is to explore alternative approaches to digital calibration of time-interleaved analog-to-digital converters.

I would like to thank my supervisor Professor Lars Lundheim for his continuous help during the course of this project. His constructive feedback, assistance in navigating the myriad of related literature, and general nudging in the right direction has been a great help. Additional thanks goes to my co-adviser Sigve Tjora for his help in formulating a specific field of study, as well as enlightening discussions concerning the topic at hand.

Kai Erik Hoff
June 19, 2014

Contents

Abbreviations

ADC	**A**nalog-to-**D**igital **C**onverter
DAC	**D**igital-to-**A**nalog **C**onverter
FD	**F**ractional **D**elay
FIR	**F**inite **I**mpulse **R**esponse
LMS	**L**east **M**ean **S**quares
MAP	**M**aximum **A** **P**osteriori
MUX	Multiplexer
PDF	**P**robability **D**ensity **F**unction

Symbols

A	Offset
G	Gain
$\bar{x}(n)$	Average of any variable 'x' over n samples
$\hat{x}(n)$	Estimate of any variable 'x' given n samples
μ_x	Mean value of a variable 'x'
σ_x	Standard deviation of a variable 'x'
$w(n)$	Random binary sequence with a variance of 1 and zero mean
$E(x)$	Expected value
F	Physical frequency
F_s	Sampling frequency
f	Normalized frequency
$\epsilon(n)$	Error signal

Chapter 1

Introduction

In digital communication, the data transfer rate between two points over an analog channel is of great concern. This transfer rate is governed by an upper limit described by Shannon's Law, which directly links the maximum achievable transfer rate to the available signal bandwidth as well as signal-to-noise ration (SNR).

As such, increasing signal bandwidth is a desirable objective. However, since the signal needs to be converted into digital information the signal bandwidth is subject to a limitation of it's own. According to the Nyquist sampling theorem the signal bandwidth cannot exceed $\frac{F_s}{2}$, where F_s is the sampling frequency, if sufficient information to recreate the recorded signal is to be collected.

Sampling an analog signal at a rate F_s requires an analog-to-digital converter (ADC) which can operate at a clock rate F_s. Once the sampling frequency enters the GHz range such components become considerably more difficult and/or expensive to make. Therefore, alternative methods of collecting sample information at the desired rate need to be explored.

One relevant technique for sampling at higher rates is time-interleaving. The basic principle is a simple one; with M ADC's taking samples at times separated by the sampling period T_s, each ADC will only need to take samples at a rate of F_s/M in order to record a digital signal with sampling frequency F_s. A diagram of this principle is shown in Figure 1.1.

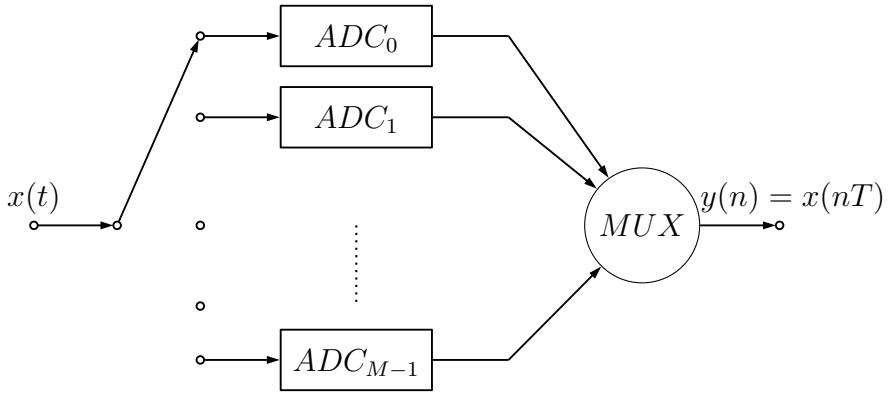

FIGURE 1.1: M Time-Interleaved ADCs.

However, by interleaving multiple ADCs certain problems are introduced. A single ADC does not take perfect measurements, and the sampled discrete time signal will be affected by Offset, Gain and Timing Offset. The mathematical relation between the continuous-time input signal $x(t)$ and the sampled discrete time signal $y[n]$ is described by

$$y[n] = G \cdot x(nT_s + \Delta_t) + A \tag{1.1}$$

where A is the Offset, G is the Gain Factor and Δ_t is the Timing Offset. A diagram of an ADC is shown in Figure X.

When the model is applied to a system consisting of M interleaved ADCs, each of the output signals $y_i[m]$ will be given by

$$y_i[m] = G_i \cdot x((M \cdot m + i)T_s + \Delta_i) + A_i, \quad i \in [1, M], \tag{1.2}$$

with M different sets of Offset, Gain and Timing Offset. m denotes the sample number for the downsampled signals with sample rate $\frac{F_s}{M}$.

When each of the signals $y_i[m]$ are put together to create a fullrate signal $y[n]$, the presence of M different Offset, Gain and Timing Offset values will distort the sampled signal. In order to recreate the optimal signal $x(nT_s)$, the precise distortion effects need to be estimated and removed from the sampled signals $y_i[m]$, $i \in [1, M]$.

1.1 Previous Scientific Work

The impact of ADC mismatches is described in detail in Vogel [2005]. Disregarding distortion from Timing mismtach for the moment, the distortion from Offset can best be described as a periodic sequence repeating itself every M samples embedded in the received signal. A fourier transform of the sampled signal will reveal the Offset distortion as spikes in the frequencies

$$f = \frac{k}{M}, k \in \{0, 1, ..., M-1\}. \tag{1.3}$$

Gain mismatch on the other will multiply a similar periodic sequence with the sampled input signal. Since the repeating Gain sequence also consists of M signal components with the frequencies in Equation (1.3), a image of the input signal will appear centered around each of the frequencies in Equation (1.3). An example of the spectral content of a Sine signal sampled with Gain and Offset mismatch is shown in Figure 1.2.

Various methods for removing this distortion have been suggested. This thesis focuses on a selection of Gain Calibration approaches which can be categorized as blind or semi-blind. One is presented in [Fu et al., 1998], and relies on embedding a known weak analog signal with the received signal which be measured once sampled.

Another approach mentioned in Jamal et al. [2002] is based on calculating the sampled energy in each subchannel, and comparing them with each other. The intended result is that one subchannel serves as reference for the other $M-1$ subchannels, which are gradually scaled to match.

Finally, a more complex method of calibrating mainly Timing mismatch but which can be modified to work for Gain calibration is presented in Huang and Levy [2006] and futher explored in Huang and Levy [2007]. This approach uses a oversampled input signal, so the sampled discrete-time signal has a narrow high-frequency band which will only contain signal components if there are mismatches between the ADCs.

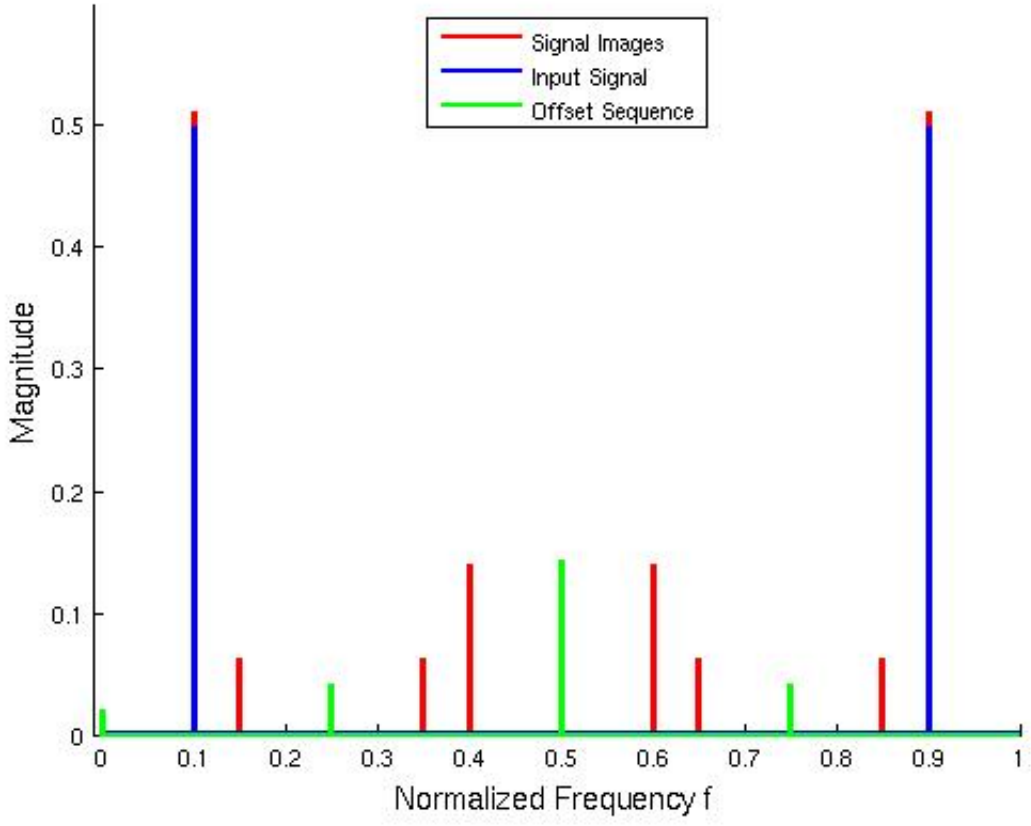

FIGURE 1.2: Spectral content of a Sinusoidal signal sampled with four interleaved ADCs.

1.2 Motivation

The main areas of focus of this thesis are methods of calibrating Gain and Offset mismatches. The effects of Timing Offset are assumed to be removed from the signal before sampling by means of an analog Trace and Hold circuit operating at full sample rate. Figure 1.3 shows a diagram incorporating this principle. The signal $w[m]$ is a random binary sequence which when multiplied with the input will result in an approximately white signal being fed to each ADC, regardless of the spectrum of $x(t)$. This process is referred to as chopping.

It is desirable to make use of a system which is capable of estimating the ADC's coefficients without needing to take the ADC(s) offline. Therefore, calibration techniques which can function while receiving a relatively unknown signal are of

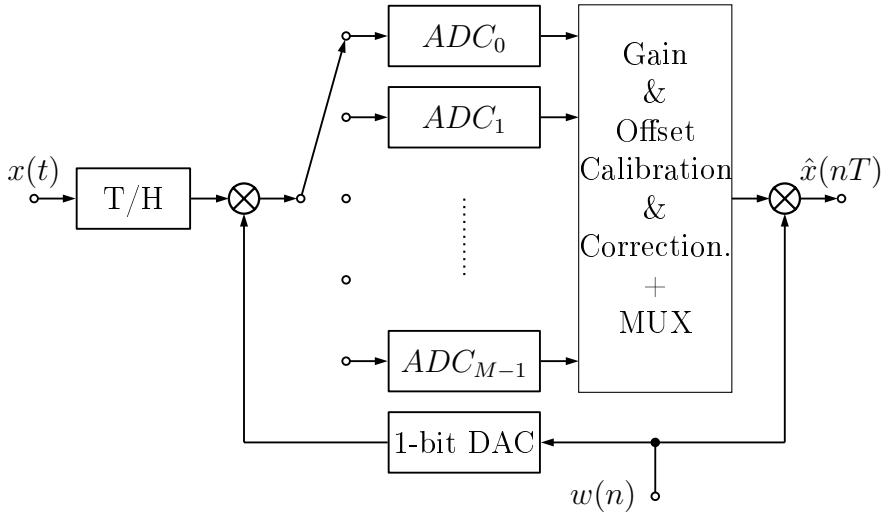

FIGURE 1.3: General interleaved ADC's with chopping.

particular interest. Such systems are known as blind calibration systems, and the methods mentioned above offer various semiblind or completely blind solutions.

By conducting a detailed analysis as well as extensive testing of the various calibration methods available a decent idea of the possibilities should emerge. The calibration methods discussed also provide possibilities for modifications, the effects of which should be thoroughly explored.

1.3 Main Contributions

Chapter 2 analyzes a simple method for calibrating Offset mismatch. A simple method of improving the efficiency of the calibration system based on a Maximum A Posteriori(MAP) estimator is introduced as an alternative to the the method stated in the original reference literature. In addition, a detailed study into best case distortion levels in relation to available sampling bits is conducted.

Chapter 3 analyzes a method for calibrating Gain mismatch involving embedding a training sequence in the received signal. A more efficient solution implementing the approximate equivalent of a MAP estimator is suggested, and the system's effectiveness is thoroughly researched.

Chapter 4 is based on a calibration system which relies on estimating the deviation in signal power between the various ADC outputs. The system is modified in order to encompass any possible number of interleaved ADCs, and various techniques aimed at increasing efficiency are researched alongside the limitations to performance based on available sampling bits.

Chapter 5 presents a modification of a more complex approach which has mainly been used for calibrating Timing Offset. The system is presented in a form which will function for any even number of ADCs, contrary to being limited to 4 ADCs in the source literature.

1.4 Outline of Thesis

Chapter 2 provides two different approaches to calibrating Offset, provided a chopped input signal. Results and discussion regarding Offset calibration is included in this chapter.

Chapter 3 presents two approaches to Gain calibration which are closely related to the Offset calibration methods. Test results from numerical simulations and discussion pertaining to the calibration approach in question is included.

Chapter 4 contains a thorough analysis of a Gain calibration method based on estimating subchannel power, as well as directly related test results and discussion.

Chapter 5 investigates the final Gain calibration method which relies on an oversampled input signal. Results and discussion specifically related to the relevant Gain calibration method are included as well.

Chapter 2

Offset

2.1 Basic Calibration Method

Considering an ADC which adds an unknown Offset of value A to the sampled signal as given as

$$y_i[m] = x((Mm + i) \cdot T_s) + A_i, \tag{2.1}$$

removing the Offset a relatively simple operation. Because the Offset will be present regardless of the input signal, averaging the signal $y_i[m]$ should produce a decent estimate of A_i as long as $x((Mm + i) \cdot T_s)$ is zero mean. This applies to any signal which does not contain one or more sinusoidal components with the normalized frequency

$$f \in \frac{k}{M}, \quad k \in \mathbb{Z}\,. \tag{2.2}$$

The absence of such signal components can be guaranteed by chopping the input signal.

Calculating the average of $y_i[m]$ over a fixed number of samples can require large amounts of memory. Instead, the values A_i can be estimated using a set of simple first-order allpole low pass filters with a very low cutoff frequency. An example of such a filter is given by the following function, where μ_A is referred to as the step

size.

$$\hat{A}_i[m+1] = y_i[m] \cdot \mu_A + (1 - \mu_A) \cdot \hat{A}_i[m] \tag{2.3}$$

Subtracting $\hat{A}_i[m]$ from the sampled signal $y(n)$ produces an estimate of $x((Mm+i) \cdot T_s)$. The filter is a single-pole filter with it's pole in $z = (1 - \mu_A)$, where the step size μ_A with a value $0 < \mu_A << 1$.

Figure 2.1 shows a diagram of an implementation of the Offset calibration system. The system is referred to as a calibration loop, and can be applied independently to each of the M ADC outputs. This approach can be found in multiple articles on the subject, but is sufficiently rudimentary to not warrant citations.

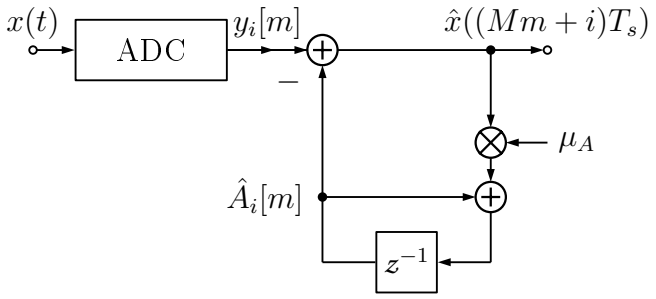

FIGURE 2.1: Basic offset calibration loop

2.2 Convergence Analysis

The step response of the filter determines how the estimates $\hat{A}_i[m]$ converge with the values A_i. This step response can be found by taking the expected value of Equation (2.3) which can be expanded to a geometric series, finally producing the equation

$$E(\hat{A}_i[m]) = A_i - (A_i - \hat{A}_i[0]) \cdot (1 - \mu_A)^m. \tag{2.4}$$

By defining $|A - E(\hat{A}[m])| < \Delta_A$ as a requirement for convergence, the number of samples needed for this condition to be fulfilled is given by the following equation.

$$m_{conv} > \frac{log(\Delta_A) - log(|A - \hat{A}[0])|}{log(1 - \mu_A)} \tag{2.5}$$

Another interesting property of the system is the estimator variance which determines the distortion caused by deviation between the actual Offset value and the Offset estimate once the two converge. By defining the estimator variance as $Var(\hat{A}_i[m]) = E(\hat{A}_i[m] - E(\hat{A}_i[m]))^2$, Equation (2.3) and Equation (2.4) can be combined to produce a expression for the variance in steady state.

$$\lim_{m\to\infty}(Var(\hat{A}_i[m])) = \frac{\sigma_x^2 \cdot \mu_A}{2 - \mu_A} \tag{2.6}$$

Equations (2.6) and (2.5) imply a trade-off between convergence time and estimator accuracy, because both of these properties depend on the step size μ_A. The estimator variance is proportional to the step size μ_A, while the convergence time is disproportionate and will approach infinity as estimator variance approaches zero.

2.3 Prior Knowledge Estimation

Because of the limitations to the system given by Equation (2.3) there may be considerable benefits to adopting alternative approaches. One relevant concept is a Maximum A Posteriori (MAP) estimator which is explained in Kay [1993]. If the probability distribution of the Offset values A_i is known, a MAP estimator combine this prior knowledge and the sample information to produce a close to optimal estimate.

The Offset values are assumed to be distributed according to a Gaussian Distribution with the probability distribution function

$$P(A) \sim \mathcal{N}(0, \sigma_A), \tag{2.7}$$

where σ_A is the Offset standard deviation. While the distribution of the sampled signal $y[m]$ is unknown, the inclusion of chopping guarantees it is uncorrelated and

approximately white. Additionally, the Central Limit Theorem permits assumptions regarding the average $\bar{y}_i[m] = \frac{1}{m}\sum_{k=1}^{m} y_i[k]$ given a sufficiently large number of available samples m.

Since the Offset value A remains practically constant, the number of samples available for estimation may be fairly unlimited. Therefore, it is reasonable to assume the average $\bar{y}_i[m]$ will have a Gaussian Distribution with the probability distribution function

$$P(\bar{y}_i[m]|A_i) \sim \mathcal{N}(A_i, \frac{\sigma_y}{\sqrt{n}}), \tag{2.8}$$

where σ_y is the standard deviation of the sampled signal.

By combining Equation (2.7) and Equation (2.8), Bayes' Theorem can be applied to find the new PDF of A_i once all the signal samples have been taken into account. The most likely value of A_i according to this PDF will be the MAP estimate and is given by Equation 2.9.

$$\hat{A}_i[m] = max(P(A_i|\bar{y}_i[m])) = \bar{y}_i[m] \cdot \frac{\sigma_A^2 \cdot m}{\sigma_y^2 + \sigma_A^2 \cdot m} + \hat{A}_i[0] \cdot \frac{\sigma_y^2}{\sigma_y^2 + \sigma_A^2 \cdot m} \tag{2.9}$$

Even though σ_y^2 is unknown, it is possible to assign a upper limit. Since the operational range of the ADC is between $-1V$ and $1V$, a reasonable upper limit to signal energy is $\sigma_y^2 < \frac{1}{2}V$, the energy of a sine wave with amplitude $1V$. A signal with more energy will most likely be severely distorted by clipping and therefore unsuitable for calibration, let alone information transfer.

An approach to implementing the MAP estimator with minimal penalty to the system's complexity is explained in Appendix A. By replacing the constant step size μ_A with the time varying step size

$$\mu_A[m] = \frac{1}{\frac{\sigma_y^2}{\sigma_A^2} + m} \tag{2.10}$$

and setting the initial Offset estimates $\hat{A}_i[0] = 0$, $i \in [1, M]$, the calibration system will produce the MAP estimate over m samples. In order to retain some tracking capability, a lower limit for $\mu_A[m]$ should be assigned. That way, the estimator reverts to the basic form in Equation (2.3) once the estimates $\hat{A}_i[m]$ are in the vicinity of the ideal values A_i.

2.4 Quantization

Up until now, the calibration method has been presented using precise mathematical definitions. Sampling is however, generally done with fixed point binary numbers with a relatively low number of bits. Signal samples are represented with b_y bits and confined to the range $-1 \leq y_i[m] < 1$. The estimated offset value $\hat{A}_i[m]$ on the other hand should be represented with enough bits to avoid significant loss of precision when multiplying $\hat{x}_i[m]$ by the step factor μ_A.

To make things simple, the step size μ_A is restricted to the set of values

$$\mu_A = 2^{-l}, \quad l \in \mathbb{Z}. \tag{2.11}$$

As a result, the act of multiplying by the step size is equivalent to a bitwise right shift of l bits. In this case, the maximum number of bits required to represent the resulting value without loss of precision is given by Equation (2.12).

$$b_{MAX} = b_y + l \tag{2.12}$$

Assuming the Offset estimate is represented with at least b_{MAX} bits, there are two instances where rounding, and thus the introduction of quantization error, occur. One quantization error sequence $\nu_{i1}[m]$ is introduced by sampling of the input signal $x(t)$ with fixed precision. Another sequence $\nu_{i2}[m]$ is introduced when $\hat{A}_i[m]$ is truncated to b_y bits in order to subtract from the sampled signal.

A diagram of the Offset calibration loop including the quantization error sequences is shown in Figure 2.2.

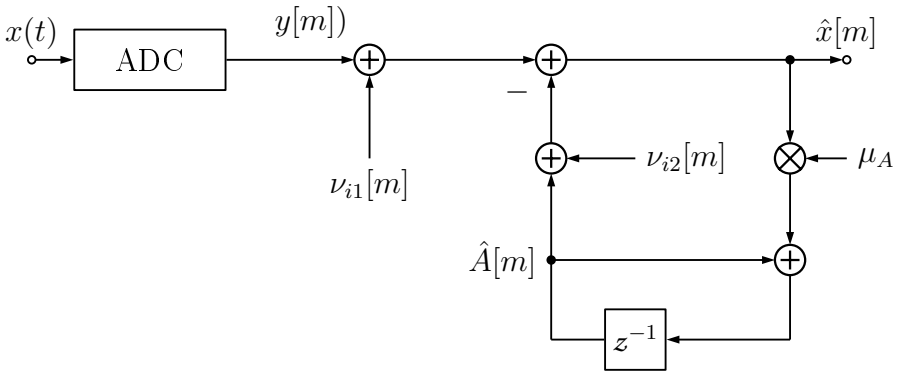

FIGURE 2.2: Basic offset calibration loop

Taking quantization error into account, the update function for $\hat{A}_i[m]$ as given by Equation (2.3) needs to be modified in order to include the introduction of quantization error, resulting in Equation (2.13).

$$\hat{A}_i[m+1] = (y_i[m] + \nu_{i1}[m] - \nu_{i2}[m]) \cdot \mu_A + (1 - \mu_A) \cdot \hat{A}_i[m] \tag{2.13}$$

The consequence of this is, even with perfect offset calibration, there will always be a residue Offset in the range $-\frac{\Delta_q}{2} < A - \hat{A}_i[m] < \frac{\Delta_q}{2}$, where Δ_q is the quantization step size given by

$$\Delta_q = 2^{-b_y+1}. \tag{2.14}$$

Since the calibration system is linear, the Offset estimate can be presented as the sum of $y_i[m]$, $\nu_{i1}[m]$ and $\nu_{i2}[m]$ passed through the calibration loop separately, as follows.

$$\hat{A}[m] = y[m] * h_A[m] + \nu_{i1}(n) * h_A[m] - \nu_{i2}[m] * h_A[m] \tag{2.15}$$

The quantization noise ν_{i1} can be assumed to be white uncorrelated noise with a uniform probability distribution

$$\nu_{i1} \sim \mathcal{U}(-\frac{\Delta_q}{2}, \frac{\Delta_q}{2}), \tag{2.16}$$

assuming clipping does not occur. $\nu_{i2}[m]$ on the other hand is the error after quantization of the Estimate $\hat{A}_i[m]$, and since $\hat{A}_i[m]$ is highly correlated with itself, $\nu_{i2}[m]$ can neither be white nor uncorrelated. Still, any possible value of $\nu_{i2}[m]$ is equally probable, as long as the signal $y_i[m]$ remains unknown, meaning ν_{i2} is initially uniformly distributed according to

$$\nu_{i2} \sim \mathcal{U}(-\frac{\Delta_q}{2}, \frac{\Delta_q}{2}), \tag{2.17}$$

The effect of $\nu_{i1}(n)$ on $\hat{A}(n)$ will be minimal, seeing as the calibration system applies a extremely narrow lowpass filter to an already weak broadband sequence. $\nu_{i2}(n)$ on the other hand is capable of manifesting as a constant value, and therefore may not lose any significant spectral power when filtered by the calibration system.

Taking this into account, the best offset calibration we can hope to achieve will still leave ν_{i2} present to distort the signal. This presents a lower limit for estimator precision, and in combination with Equation (2.6) a lower limit where decreasing the step size μ_A further will have negligible effect on the distortion levels.

If $\mathbb{Q}$ is the set of 2^b possible sample values, and A_q is the value in $\mathbb{Q}$ closest to the actual Offset value A, then the smallest possible distortion of the signal is $A - A_q$. Since the value A is unknown, the best that can be done is assume $A - A_q$ will be uniformly distributed between $-\frac{\Delta_q}{2}$ and $\frac{\Delta}{2}$. On average, this distortion can be expected to have a power given by Equation (2.18).

$$E((A - A_q)^2) = \frac{\Delta_q^2}{12} = \frac{2^{-2b_y}}{3} \tag{2.18}$$

If the estimator variance is less than $\frac{2^{-b_y}}{3}$, the distortion effect from estimator inaccuracy will be overshadowed by the quantizatin errors ν_{q1} and ν_{q2}. Assuming once again that $\sigma_x^2 < \frac{1}{2}$, combining Equation (2.18) and (2.6) presents the step size in Equation (2.19) resulting in distortion effect smaller than the quantization noise. The step size μ_A is chosen to be among the values given by Equation (2.11).

Bits per Sample	Constant Step Size	MAP Estimator
8	$8.82 \cdot 10^4$	$6.31 \cdot 10^3$
10	$2.86 \cdot 10^6$	$3.19 \cdot 10^4$
12	$6.91 \cdot 10^7$	$1.34 \cdot 10^5$
14	$1.48 \cdot 10^9$	$5.44 \cdot 10^5$
16	$2.96 \cdot 10^{10}$	$2.18 \cdot 10^6$

TABLE 2.1: Convergence times for step sizes tuned for minimum steady-state distortion

$$\mu_A = 2^{-2b_y} < \frac{4}{3} \cdot 2^{-2b_y} \tag{2.19}$$

By using Equation (2.5) and setting $\Delta_A = 2^{-b_y}$, the expected number of samples required for the SNDR to reach it's minimum level is found to be given by Equation (2.20). Similarly, the corresponding number of samples required when using the MAP estimator in Equation (2.9) is given by Equation (2.21).

$$E(n_{conv}) > \frac{b_{sig} - log_2(\sigma_A)}{log_2(1 - 2^{-2b_y})} \tag{2.20}$$

$$E(n_{conv}) > \frac{1}{2\sigma_A^2} \cdot \left(\frac{\sigma_A}{2^{-b_y}} - 1\right) \tag{2.21}$$

Table 2.4 shows the theoretical convergence time for various sample resolutions.

2.5 Simulation Setup and Results

The calibration system is tested multiple times using randomly generated Offset values. Offset standard deviation is set to $\sigma_A = 0.015V$, and simulations are conducted assuming $M = 4$ interleaved ADCs. Estimator convergence is tested using both Additive White Gaussian Noise (AWGN) and sinusoidal signals as input, and AWGN input is used to find more extensive data concerning the Mean Square Error(MSE) of the estimator given sample number m.

The approximate MSE sequences are considered in relation to the minimum obtainable MSE according to theory $E(J_{min}[m]) = 2 \cdot \frac{\Delta_q^2}{12} = E((\nu_{i1}[m] + \nu_{i2}[m])^2)$. Multiple different sample resolutions are used.

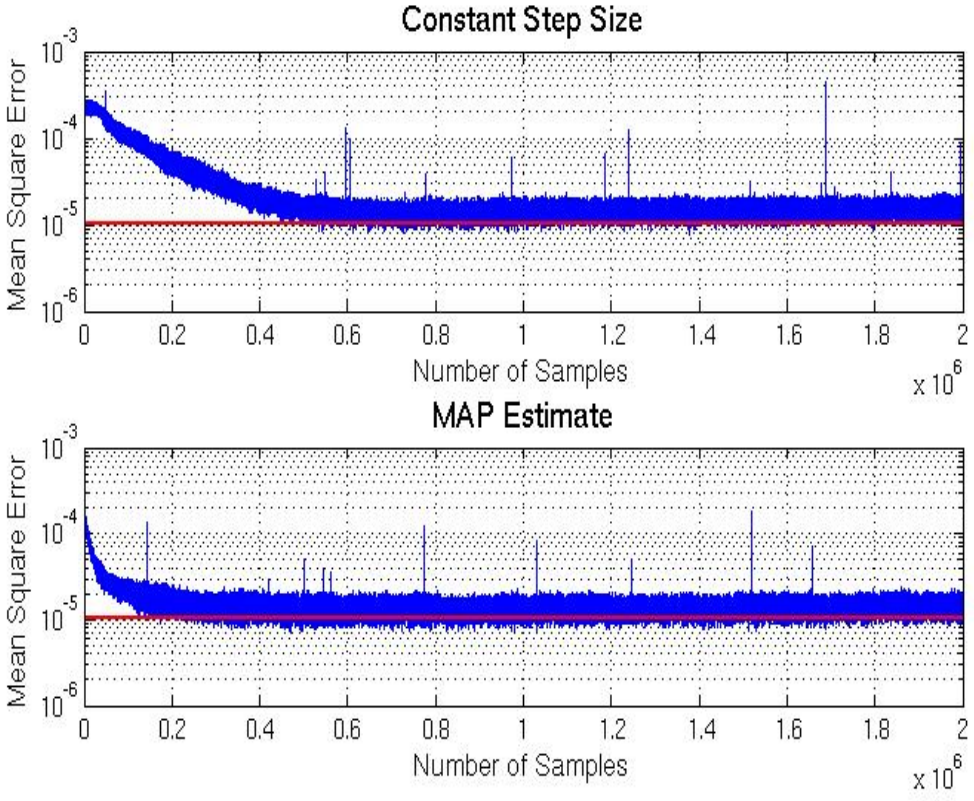

FIGURE 2.3: Mean square error for MAP and fixed step size estimator with $b_y = 8$ and $\sigma_x = 0.2$ AWGN

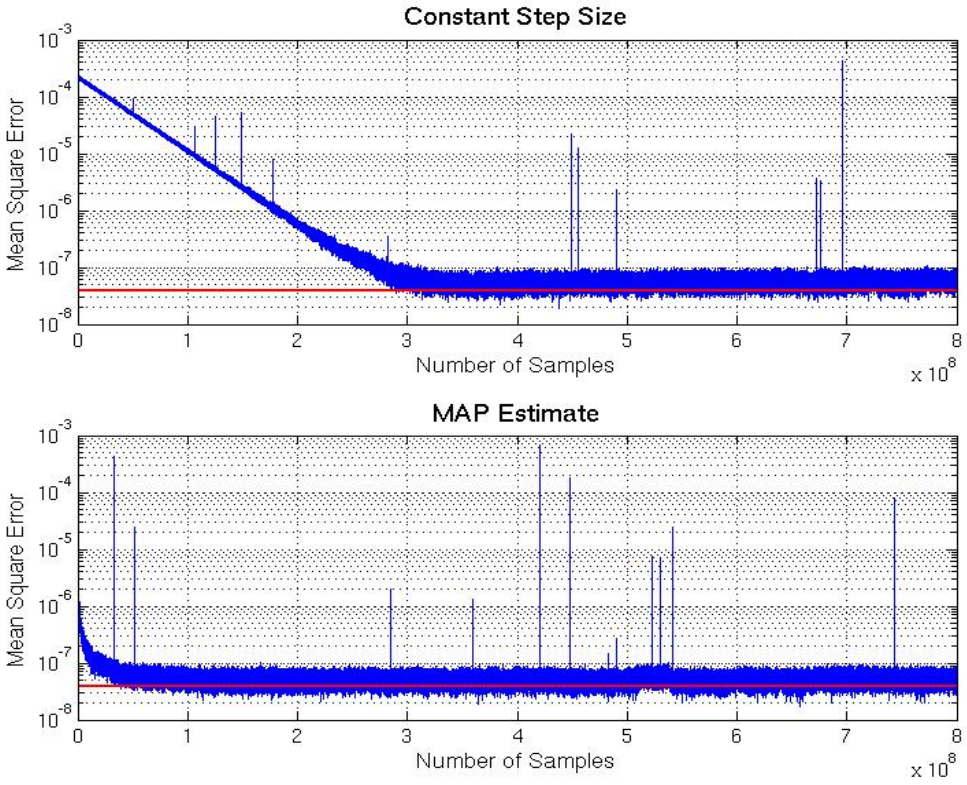

FIGURE 2.4: Mean square error for MAP and fixed step size estimator with $b_y = 12$ and $\sigma_x = 0.2$ AWGN

2.6 Discussion

2.6.1 Stability

The results in Section 2.5 show the Offset estimate is stable regardless of the input signal. This holds true for the MAP-based Offset estimator as well. Chopping the input signal ensures uncorrelated samples, guaranteeing that the only correlation present is caused by the Offset.

2.6.2 Performance

Figures X and Y show the average square error over 50 different and independent simulations. The average square error is not far removed from the ideal distortion

level marked by the red line, except occasional spikes which are likely caused by the clipping.

The results confirm that the MAP-estimator produces a much higher rate of convergence than the constant step size. Figures ?? and ?? show that the standard algorithm reaches a steady MSE after approximately $n = 2 \cdot 10^8 \frac{1}{M}$ samples. The MAP estimator reaches the same level of MSE after approximately $n = 5 \cdot 10^7 \frac{1}{M}$ samples. This fits nicely with the theoretical values in Table 2.4.

Chapter 3

Gain Calibration by Using a Training Sequence

3.1 Calibration Algorithm

This chapter considers a set of interleaved ADCs which multiply the sampled signal by a corresponding set of unknown Gain factors G_i, $i \in [1, M]$. A technique presented in Fu et al. [1998] is somewhat similar to the Offset calibration method in Chapter 2. By adding a known random binary sequence $w_2[m]$ attenuated by a constant value k to the input signal before sampling, each of the ADC outputs $y_i[m]$ can be described by Equation (3.1) where G_D is the Gain factor of the DAC used to convert the sequence $w_2[m]$ to an analog signal.

$$y_i[m] = G_A \cdot x((M \cdot m + i)T_s) + G_D G_A \cdot k w_2[m], \quad i \in 1..M \tag{3.1}$$

It is worth noting that the sequence $w_2[m]$, as with chopping, merely needs to change at a frequency $\frac{F_s}{M}$. The random training sequence$k \cdot w_2[m]$ can be identical for each subchannel signal $y_i[m]$, as long as the sequence embedded in each individual subchannel remains uncorrelated.

Once the random binary training sequence is embedded in the input signal, the Gain factor of each ADC can be independently determined by means of the error signals $\epsilon_i[m]$ given by Equation (3.2).

$$\epsilon_i[m] = (y_i[m] \cdot \hat{G}_i[m] - k \cdot w_2[m])w_2[m] \tag{3.2}$$

Some trace of $w_2[m]$ will be present in $\epsilon_i[m]$ if the corresponding Gain estimate $\hat{G}_i[m]$ is not properly estimated. This error signal can be used by a simple LMS algorithm, see J. G. Proakis [2008], where the values $\hat{G}_i[m]$ are updated according to Equation (3.3) with μ_G denoting the step size.

$$\hat{G}_i[m+1] = \hat{G}_i[m] - \epsilon_i[m] \cdot \mu_G \tag{3.3}$$

The algorithm is easily implemented as shown in Figure 3.1, and can be applied independently to each ADC output.

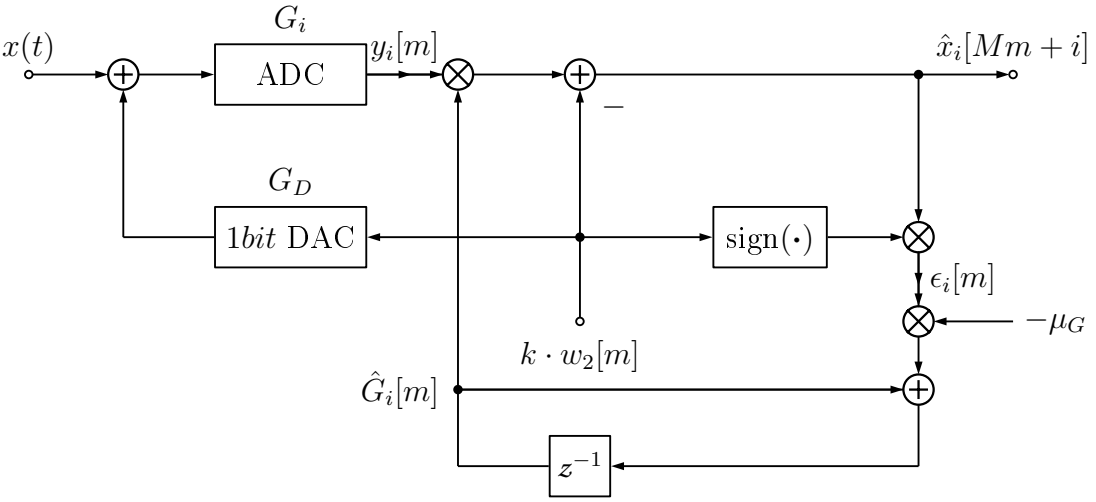

FIGURE 3.1: Gain calibration loop using random training sequence

3.2 Convergence Analysis

In order to further study the behavior of the Gain calibration system, Equations (3.1), (3.2) and (3.3) are combined to produce Equation (3.4) which includes all the variables the estimates $\hat{G}_i[m]$ are dependent on.

$$\hat{G}_i[m+1] = \mu_G \cdot k - x[Mm+i]\mu_G w_2[m] G_i \cdot \hat{G}_i[m] + (1 - \mu_G k G_D G_i) \cdot \hat{G}_i[m] \quad (3.4)$$

The expected value $E(\hat{G}_i[m])$ determines how $\hat{G}_i[m]$ converges with the inverse gain factor $(G_i G_D)^{-1}$. $E(\hat{G}_i[m])$ is found by recursively expanding Equation (3.4), producing a geometric series which ultimately yields Equation (3.5).

$$E(\hat{G}_i[m]) = \frac{1}{G_i G_D} - \left(\frac{1}{G_i G_D} - \hat{G}_i[0] \right) \cdot (1 - \mu_G k G_D G_i)^m \quad (3.5)$$

As in Chapter 2, the expression in Equation (3.6) for the calibration time is found by using Equation (3.5) and defining $|(G_D G_A)^{-1} - E(\hat{G}[m])| < \Delta_G$ as a requirement for convergence.

$$m_{conv} > \frac{\log(\Delta_G) - \log((G_D G_i)^{-1} - \hat{G}[0])}{\log(1 - \mu_G k G_D G_i)} \quad (3.6)$$

Similarly, Equations (3.4) and (3.5) are used to acquire Equation (3.7) describing estimator variance when the estimate is in steady state.

$$\lim_{m \to \infty} (Var(\hat{G}_i[m])) = \frac{\mu_G \sigma_x^2}{2 G_D G_A - \mu_G k^2 G_D^2 G_A^2} \quad (3.7)$$

As with the Offset estimation in Chapter 2, there is a significant tradeoff between estimate certainty and the number of samples required for the estimates to converge.

3.3 Prior Knowledge Estimation

Assuming the Gain factors have a Gaussian PDF with variance $Var(G_i) = \sigma_G^2$, a MAP Estimator for the Gain factors $G_i G_D$ can be found by using the error signal given by Equation (3.2). Given a chopped input signal, the average of the error signal $\bar{\epsilon}(n)$ can be assumed to have a Gaussian probability distribution described by Equation (6).

$$P(\bar{\epsilon}(n)|G_D G_A) \sim \mathcal{N}(G_D G_A - 1, \frac{\sigma_x^2}{\sqrt{n}}) \tag{3.8}$$

$$Var(G_A G_D) = 2\sigma_G^2 + \sigma_G^4 \tag{3.9}$$

Bayes' Theorem and Equations (6) and (7) combined produce a MAP estimator for the gain factor $G_D G_i$ given by equation (8)

$$\hat{G}_i[m] = max(P((G_i G_D)|\bar{\epsilon}_i(m))) = \frac{\bar{\epsilon}(n) \cdot n}{\frac{\sigma_x^2}{2\sigma_G^2 + \sigma_G^4} + m \cdot k} + 1 \tag{3.10}$$

As shown in Appendix A, an approximation to the MAP estomator can be implemented by applying a gradually decreasing step factor

$$\mu_G[m] = \frac{1}{\frac{\sigma_x^2}{2\sigma_G^2 + \sigma_G^4} + m \cdot k} \tag{3.11}$$

and setting the initial Gain estimates $\hat{G}_i[0] = 1$. This approximation does not result in any significant deviation from the actual MAP estimator for the vast majority of possible Gain mismatches.

3.4 Quantization

For the purpose of gain calibration, the gain estimate should be in the range $0 \leq \hat{G}_i[m] = 2$. Apart from this deviation from the setup in Chapter 2, fixed-point values are handled in the same manner. That is to say, $y_i[m]$ represented with b_y bits, and the Gain estimates are represented with at least $b_y - \log_2(\mu_G)$ bits where $\log_2(\mu_G) \in \mathbb{Z}$.

Assuming the value k deciding the amplitude of the training sequence can be represented using b_y bits with fixed point representation, there will be three instances of added quantization noise. Firstly, sampling the signal $x(t)$ with finite precision adds the quantization error $\nu_{i1}[m]$. Multiplying the sampled signals $y_i[m]$ with the current Gain estimates will introduce the quantization error $\nu_{i2}[m]$, and trunctating the Gain estimates $\hat{G}_i[m]$ to b_y bits introduces the error $\nu_{i3}[m]$.

The various sources of quantization error are included in a diagram of the system in Figure 3.2. For the moment, distortion introduced by Offset calibration which occurs before Gain calibration is not taken into account.

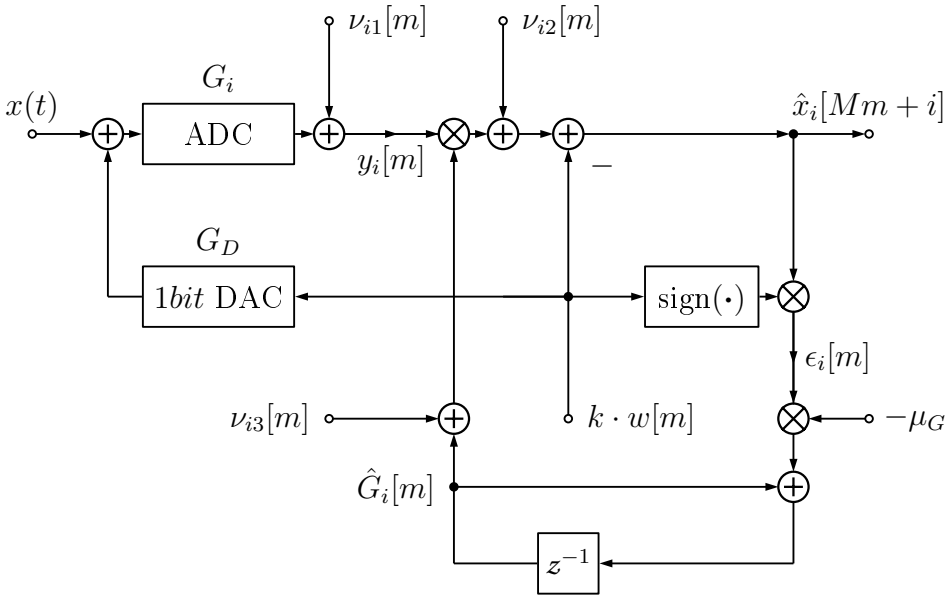

FIGURE 3.2: Gain calibration loop using random training sequence

The quantization errors $\nu_{i1}[m]$ and $\nu_{i2}[m]$ will be white and uncorrelated, with a uniform PDF $P = \mathcal{U}(-\frac{\Delta_q}{2}, \frac{\Delta_q}{2})$. Since the Gain estimates are also in principle

found using a very narrowband lowpass filter, these error sequences will have minimal effect on the Gain estimates.

$\nu_{i3}[m]$ on the other hand cannot be as easily ignored. While it will still have a uniform PDF $P = \mathcal{U}(-\frac{\Delta_q}{2}, \frac{\Delta_q}{2})$ initially, it is produced by trunctating the Gain estimate, which is far from uncorrelated. Therefore, $\nu_{i3}[m]$ may cause some deviation in the Gain estimates.

It is possible to estimate the Gain mismatch because a Gain mismatch produces an offset value $(G_D G_i - 1) \cdot k$ in the signal $\epsilon_i[m]$. A limitation to this calibration method is the minimal offset which can be registered using b_y bits to sample the signal. This limitation is presented by Equation (3.12), which makes it clear that the precision of the estimate depends not only on the number of bits per sample, but also the amplitude of the training sequence.

$$1 - \frac{\Delta_q}{2k} < G_D G_i \hat{G}_i(n) < 1 + \frac{\Delta_q}{2k} \tag{3.12}$$

Because there is such a limitation to the calibration system's sensitivity, it is interesting to find a theoretical lower limit for μ_G where further reduction will have negligible effect on the quality of the reconstructed signal $\hat{x}[n]$. Based on the limitations described by Equation (3.12) having Gain estimates with significantly less variance than hypothetical uniformy distributed noise with PDF $P \sim \mathcal{U}(-\frac{\Delta_q}{2k}, \frac{\Delta_q}{2k})$ should be unnecessary. Based on this observation, a reasonable range for estimator variance would be

$$\frac{1}{2} \cdot \frac{2^{-2b_y}}{3k^2} < E(Var(\hat{G}_i[m])) < \frac{2^{-2b_y}}{3k^2} \tag{3.13}$$

where $E(Var(\hat{G}_i[m])) \approx \frac{\mu_G \sigma_x^2}{2}$ is approximately the expected value of Equation (3.7). By rewriting Equation (3.13) and assuming $\sigma_x^2 = 0.5$ to be a reasonable maximum signal variance, a suitable value for the step factor μ_G is described as

$$\frac{2 \cdot 2^{-2b_y}}{3k^2} < \mu_G < \frac{4 \cdot 2^{-2b_y}}{3k^2}. \tag{3.14}$$

3.5 Numerical Simulations

The calibration system is tested multiple times using randomly generated Gain values. Offset standard deviation is set to $\sigma_G = 0.05V$, and simulations are conducted assuming $M = 4$ interleaved ADCs. Estimator convergence is tested using both Additive White Gaussian Noise (AWGN) and sinusoidal signals as input, and AWGN input is used to find more extensive data concerning the Mean Square Error(MSE) of the estimator given sample number m. A training sequence of amplitude $k = 0.125$ was used to test both algorithms.

The approximate MSE sequences are considered in relation to the minimum obtainable MSE according to theory $E(J_{min}[m]) = 2 \cdot \frac{\Delta_q^2}{12}$. Multiple different sample resolutions are used.

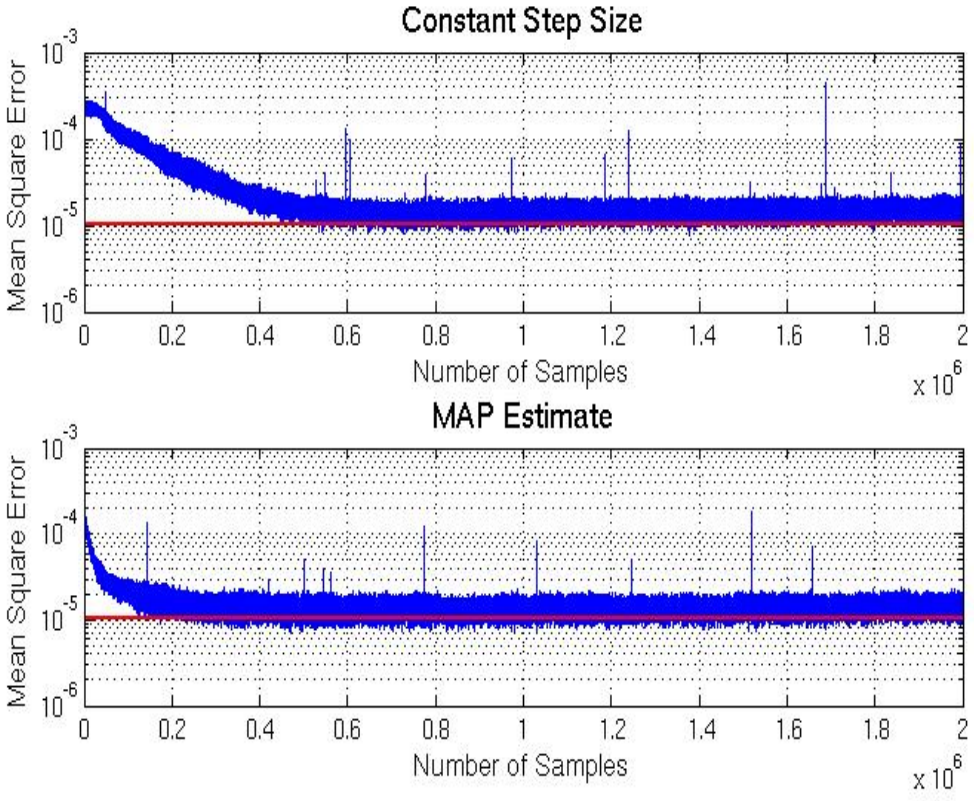

FIGURE 3.3: Mean square error for MAP and fixed step size estimator with $b_y = 12$ and $\sigma_x = 0.2$ with AWGN input

3.6 Discussion

3.6.1 Stability

This calibration method relies on a known sequence not present in the actual input signal to calibrate the gain mismatch. In addition, the sequences $\epsilon_i[m]w_2[m]$ used to update $\hat{G}_i([m]$ will be white and uncorrelated due to the random nature of the training sequence $k \cdot w_2(n)$. As a result, the algorithm will produce a stable output regardless of the input signal.

The results in Section 3.5 indicate the algorithm reacts similarly to Gaussian noise input and sinusoidal input. There are no signs of estimator instability present.

3.6.2 Performance

Figure 3.3 shows the average square error over 50 different and independent simulations. The average square error is not far removed from the ideal distortion level marked by the red line, except occasional spikes which are likely caused by the clipping.

The results confirm that the MAP-estimator produces a much higher rate of convergence than the constant step size. Figure 3.3 shows that the standard algorithm reaches a steady MSE after approximately $n = 0.6 \cdot 10^8$ samples. The MAP estimator reaches the same level of MSE after approximately $n = 0.2 \cdot 10^8$ samples.

3.6.3 Scaling

This algorithm can be applied independently to multiple ADC outputs, and the calibration loops for each ADC can all use the same training signal so only one DAC will ever be necessary.

An arrangement where one calibration corrects the mismatch between two ADCs is suggested in Fu et al. [1998] in order to minimize the required resources, but

adding more ADCs involves arranging the calibration loops in a cascade which reduces the overall convergence rate. For large numbers of ADCs, the benefit to the reduced amount of arithmetic operations will be minimal.

Chapter 4

Gain Calibration by Comparing Subchannel Power

4.1 Calibration Algorithm

While embedding a known calibration sequence in the received signal does present a reliable basis for estimating the Gain mismatches regardless of the input signal, it does come at a cost. For one, the available sampling range will need to be reduced in order to accommodate for the calibration sequence. More importantly however, it completely ignores any information concerning the Gain mismatches contained within the sampled signal itself.

One approach to calibrating Gain mismatch solely by using the input signal is presented in Jamal et al. [2002], which applies to $M = 2$ interleaved ADCs. The main principle is to find the average sample power for each subchannel, and gradually adjust the amplitude of one until the two power estimates are matched.

With a few modifications, the algorithm can be adapted to calibrate gain mismatch between any arbitrary number M of interleaved ADCs, by using one subchannel as reference for the other $M - 1$ subchannels. If we the subchannel signals $y_i[m]$

are as defined as

$$y_i[m] = G_i \cdot x((M \cdot n + i)T_s), \quad i = 1..M\ , \tag{4.1}$$

$y_1[m]$ can be used as the reference signal, and each of the other signals $y_i[m], \quad i = 2..M$ need to be scaled in order to match $y_1[m]$.

This can be done for instance by analyzing the $M-1$ error sequences defined by Equation (4.2). The mean of each error sequence will present an indication of the mismatch between G_1 and each of the values $G_2..M$. This property can be utilized to calibrate the gain mismatch by means of the algorithm in Equation (4.3), where μ_G is a sufficiently small step size to ensure the estimate will converge with the desired value. An indication of the mismatch between G_1 and each of the Gain factors $G_i,\ i \in 2..M$ can be given by

$$\epsilon_i[m] = y_1^2[m] - (y_i[m] \cdot \hat{G}_i[m])^2, \quad i = 2..M\ . \tag{4.2}$$

While $\epsilon_i[m]$ can vary greatly, the expected value of $\epsilon_i[m]$ will be proportional to $G_1^2 - G_i^2 \cdot \hat{G}_i^2[m]$, $i \in 2..M$. Thus, updating the estimates $\hat{G}_i[m]$, $i \in 2..M$ according to the function

$$\hat{G}_i[m+1] = \hat{G}[m] + \mu_G \cdot \epsilon_i[m], \quad i = 2..M \tag{4.3}$$

will over time produce a stable set of estimates, assuming the step size μ_G is sufficiently small.

Ideally, each estimate $\hat{G}_i[m]$ should converge with $\frac{G_1}{G_i}$, resulting in all subchannels being uniformly scaled to match G_1 as the number of samples n available becomes sufficiently large. As the estimates $\hat{G}_i[m]$ approach the ideal values, the expected value of $\epsilon_i[m]$ in Equation (4.2) will approach zero.

As a point of interest, the main principle of the calibration algorithm should not be altered if the sequence $\epsilon_i[m]$ is instead given as

$$\epsilon_i[m] = |y_1[m]| - |y_i[m]| \cdot \hat{G}_i[m], \quad i \in 2..M\ . \tag{4.4}$$

The expected values of $\epsilon_i[m]$ will now be proportional to $G_1 - G_i \cdot \hat{G}_i[m]$, $i \in 2..M$, which ultimately results in the same general behavior for the calibration algorithm. Because squaring the values of $y_i[m]$ is a much more demanding arithmetic operation than simply taking the absolute value, substituting Equation (4.2) with Equation (4.4) may be desirable.

Figure 4.1 shows an implementation of the calibration algorithm in Equation 4.3 with the addition of a set of filters not previously discussed. The filters $H(\omega)$ are needed in order to remove unwanted signal components prior to calibration.

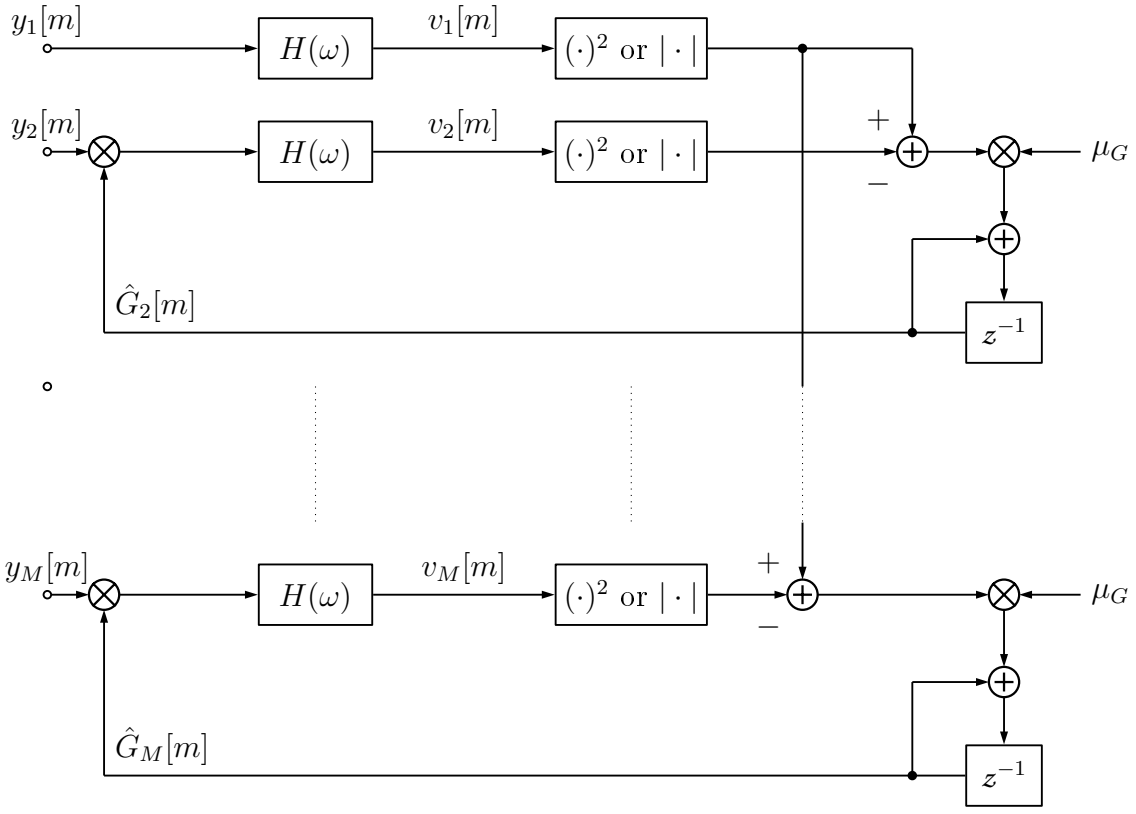

FIGURE 4.1: Calibration loop comparing subchannel average power

4.2 Harmful signal components

Because the signals $y_i[m] \in [1, M]$ are undersampled versions of the continuous signal $x(nT_s)$, aliasing will be present. This is generally not a problem except

in the cases where any signal $y_i[m]$ contains a signal component with normalized frequency $f = 0$ or $f = \frac{1}{2}$. In a system composing of M interleaved ADCs this applies to the entire set of frequencies described by Equation (4.5).

$$f_k = \frac{k}{2M}, \quad k \in [0, M] \tag{4.5}$$

Given a input signal $x(t) = cos(2\pi \cdot F_s \cdot (f + \Delta_t)), f \in f_i$, the error sequences in Equation 4.2 can be described by Equation 4.6.

$$\begin{aligned}
\epsilon_i[m] &= A^2 G_1^2 \cdot \cos^2(\pi k m + 2\pi\Delta_t) \\
&\quad - A^2 G_i^2 \cdot \cos^2\left(\pi k \left(m + \frac{i-1}{M}\right) + 2\pi\Delta_t\right), \quad i \in [2, M] \\
&= A^2 G_1^2 \cdot \left(\frac{1}{2} + \frac{1}{2}\cos(4\pi\Delta_t)\right) \\
&\quad - A^2 G_i^2 \cdot \left(\frac{1}{2} + \frac{1}{2}\cos\left(\pi k \frac{i-1}{M} + 4\pi\Delta_t\right)\right), \quad i \in [2, M]
\end{aligned} \tag{4.6}$$

Seeing as the sequences $\epsilon_i[m]$ in Equation (4.6) may be constant at any value between $A^2G_1^2$ and $-A^2G_i^2$ regardless of m, it is a extremely poor basis for estimating the Gain mismatch.

To avoid this problem, all the signals $y_i[m]$ should be filtered to remove any signal component of normalized frequency given by Equation $f = 0$ or $f = \frac{1}{2}$. A second order FIR-filter $H(z) = 0.5 - 0.5z^{-2}$ is sufficient, but [Jamal et al., 2002] do mention the possible benefit of a notch filter with a steeper slope of descent.

Since the aforementioned second order FIR filter has a total cumulative magnitude response of $\frac{1}{2}$, a lot of potentially useful signal energy will be lost to a varying degree. To that end it may be worthwhile to consider a more complex IIR-filter.

A relatively simple filter with transfer function given by Equation (4.7) has zeros in $z = \pm 1$ and poles in $z = \pm\sqrt{r}$, and has a magnitude response as given by Equation (4.8).

$$H(z) = \frac{1+r}{2} \cdot \frac{1-z^{-2}}{1-r \cdot z^{-2}}, \quad 0 \leq r < 1 \tag{4.7}$$

$$|H(\omega)|^2 = \frac{(1+r)^2}{4} \cdot \frac{2-2\cos(2\omega)}{1+r^2-2r \cdot \cos(2\omega)} \leq 1 \tag{4.8}$$

By using MATLAB to find an approximation to $\int_0^{2\pi} |H(\omega)|^2 d\omega$ for a large number of different values r, the total cumulative magnitude response of $H(z)$ is found to be consistent with Equation 4.9. Figure 4.2 shows the magnitude response of $H(z)$ for different values r.

$$\int_0^{2\pi} |H(\omega)|^2 d\omega = \frac{1}{2} + \frac{r}{2} \tag{4.9}$$

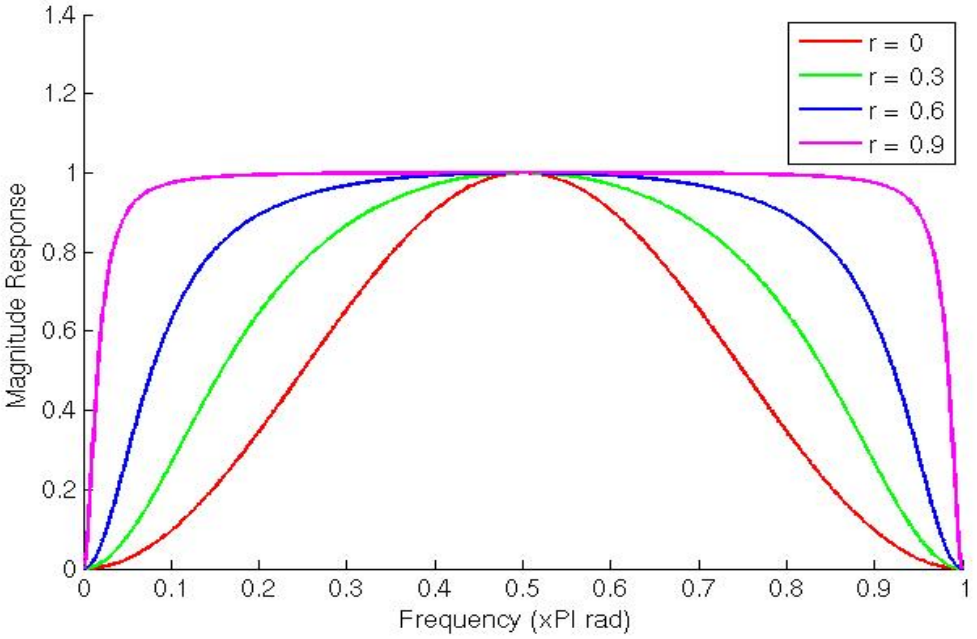

FIGURE 4.2: Magnitude Response of Various Notch Filters

4.3 Convergence Analysis

Finding a definitive function describing the convergence is difficult, because recursively expanding Equation (4.3) quickly becomes an immensely complicated

expression. However, the expected value $E(\hat{G}_i[m])$ does offer some indication as to what factors effect the rate of convergence, as well as proof that the estimate $\hat{G}_i[m]$ does converge. If the input signal is wide-sense stationary (WSS) and the notch filter $H(\omega)$ is temporarily disregarded, $E(\hat{G}[m])$ will be given by Equation (4.10).

$$E(\hat{G}_i[m+1]) = \mu_G \sigma_x^2 \cdot (G_1^2 - G_i^2 \cdot \hat{G}_i^2[m]) + \hat{G}[m] \tag{4.10}$$

Each iteration will on average modify $\hat{G}_i[m]$ by a amount proportional to the step size μ_G, the remaining uncalibrated mismatches, and the signal power σ_x^2 until $\hat{G}_i[m]$ converges with $\frac{G_1}{G_i}$. This suggests that the convergence rate is dependent on the signal power σ_x^2.

On the other hand, recursively expanding the expected value of Equation (4.3) when $\epsilon_i[m]$ is given by Equation (4.4) produces a geometric series. Thus, the expected Gain estimate for a number of available samples m when using the absolute value of $y_i[m]$ will be given by

$$E(\hat{G}_i[m]) = \frac{G_1}{G_i} - \left(\frac{G_1}{G_i} - \hat{G}_i[0]\right)(1 - \mu_G G_i E(|x(t)|))^m . \tag{4.11}$$

In order to conduct a more comprehensive comparison between the system performance with $\epsilon_i[m]$ given by Equation (4.2) and Equation (4.6) it is desirable to study the statistical properties of the two different $\epsilon_i[m]$ sequences.

Seeing as a sine wave with power $\sigma_x^2 = \frac{1}{2}$ is the most powerful input signal which can be reasonably expected, choosing parameters according to such an input signal should ensure

As an example, if the input signal $x(t)$ uncorrelated white uniformly distributed noise, Figure *Something* shows the expected Gain estimates for the Estimator in equation this and that.

By squaring the signals $y_i[m]$, a decrease in the power of $x(t)$ will

4.4 Quantization

The fixed point values in the current Gain calibration method are represented in the same manner as in Chapter 3. However, both filtering and squaring the signal will cause a degree of quantization error.

One added complication to squaring the input signal becomes evident when the product is truncated to b_y bits. The output from a multiplier will ideally be $2b_y$ bits, meaning any signal value $v_i[m] \leq 2^{-0.5 \cdot b_y}$ will be rounded off to zero once the product is truncated. For weak input signals, this may hinder the estimation process.

All told, the calibration loops will include six or four cases of rounding, depending on whether the calibration system is based on squaring or taking the absolute value of the signal respectively. A diagram showing all the potential instances of added quantization noise is shown in Figure 4.3.

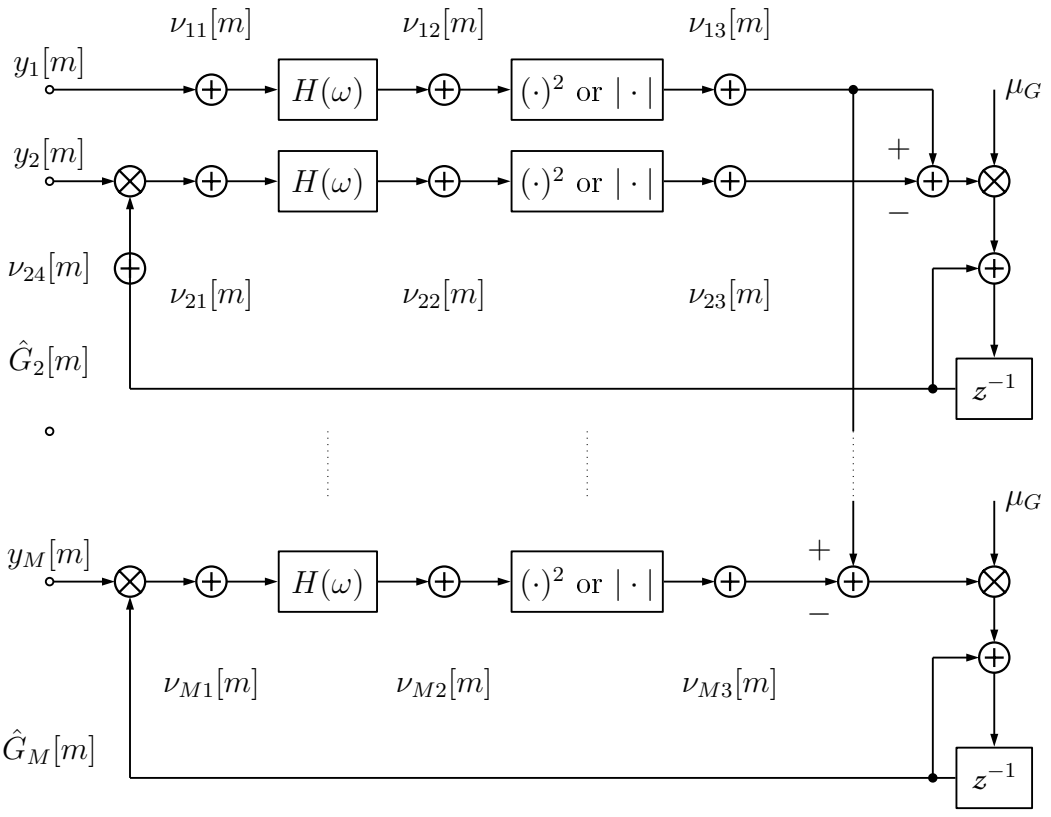

FIGURE 4.3: Calibration loop comparing subchannel average power

All of the sequences $\nu_{ij}[m]$, $i \in [1, M]$, $j \neq 4$ can be assumed to be white, uncorrelated and have a uniform PDF $P(\nu) = \mathcal{U}(-\frac{\Delta_q}{2}, \frac{\Delta_q}{2})$. $\nu_{i4}[m]$, $i \in [2, M]$ will be correlated because the Gain estimate is highly correlated. Initially however, the PDF of ν_{i4} will also be uniform $P(\nu_{i4}) = \mathcal{U}(-\frac{\Delta_q}{2}, \frac{\Delta_q}{2})$.

Since calculating the estimator variance is exceptionally difficult in this case, it is challenging to find the theoretical step size which produces a close to minimal signal distortion. Hence a suitable value for μ_G can potentially be found by means of simulation testing.

4.5 Numerical Simulations

The calibration system is tested multiple times using randomly generated Gain values. Offset standard deviation is set to $\sigma_G = 0.05V$, and simulations are conducted assuming $M = 4$ interleaved ADCs. Estimator convergence is tested using both AWGN and sinusoidal signals as input, and AWGN input is used to find more extensive data concerning the Mean Square Error(MSE) of the estimator given sample number m.

The approximate MSE sequences are considered in relation to the minimum obtainable MSE according to theory $E(J_{min}[m]) = 2 \cdot \frac{\Delta_q^2}{12} = E((\nu_{i1}[m] + \nu_{i2}[m])^2)$. Multiple different sample resolutions are used, and thus, multiple different step factors μ_G.

All the possible permutations of suggested modifications are tested, in order to illustrate their significance. That is to say, estimation based on squaring the sampled signal and averaging absolute value are both tested with and without notch filters.

4.6 Discussion

4.6.1 Stability

All four possible approaches appear to produce stable estimates $\hat{G}_i[m]$, albeit with different rates and certainty. The exception is of course when the input signal is one of the frequencies described by Equation (4.5), in which case the estimates will remain completely stationary.

4.6.2 Performance

Figures 4.5 and 4.6 illustrate the problem of the convergence rate being dependent on signal energy. When the input signal is close to $f = 0.25$ in this case, the system without a notch filter will have much less signal power available to

As seen in Figure 4.4, the system does approach the theoretical lower limit for distortion. There are a few spikes present in the MSE plots, but they are probably the result of occasional clipping. The advantage to using a notch filter is also clearly evident, as it nearly halves the calibration time for the estimate based on signal power.

4.6.3 Concurrency

Any remaining Offset still present in the signal when this algorithm is used to estimate Gain mismatch will affect the estimate. If the input signal is chopped in order to safely estimate Offset, any residue Offset will not be removed from the signal by means of the notch filters. Therefore, errors in Offset calibration will directly translate to errors in Gain calibration.

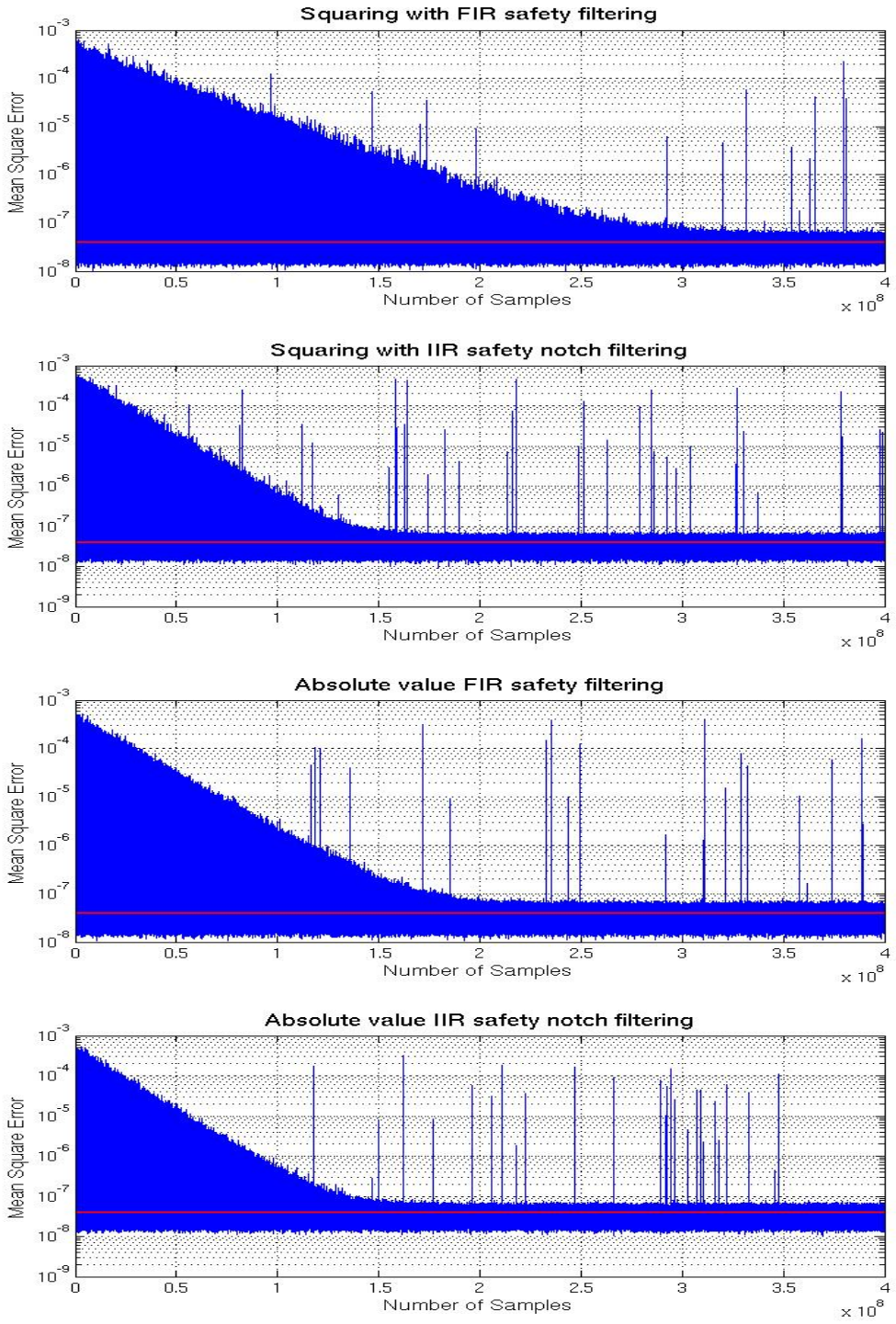

FIGURE 4.4: The average MSE of all four versions of the calibration system over 50 iterations, with $\sigma_x = 0.2$ and AWGN input signal. All the signals are sampled with $b_y = 12$ bits.

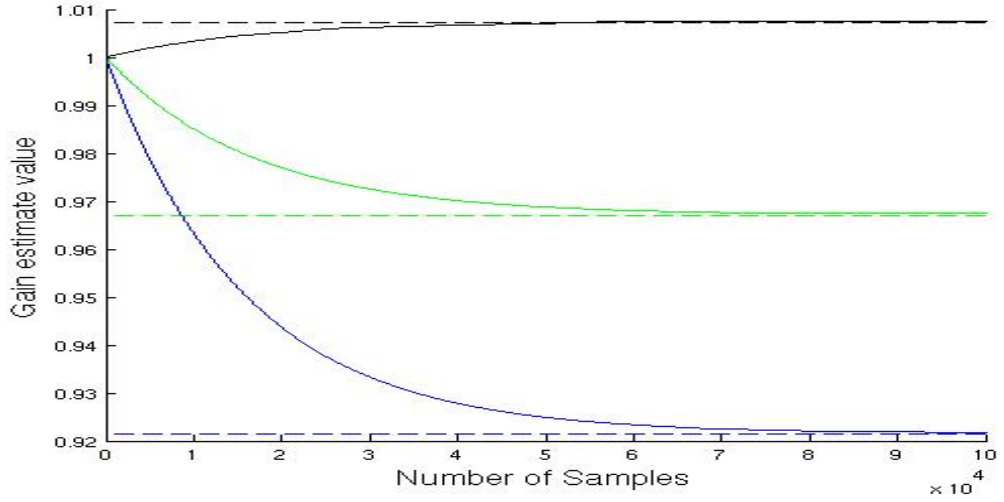

FIGURE 4.5: Convergence of Absolute value algorithm without notch filter for $f = 0.24$

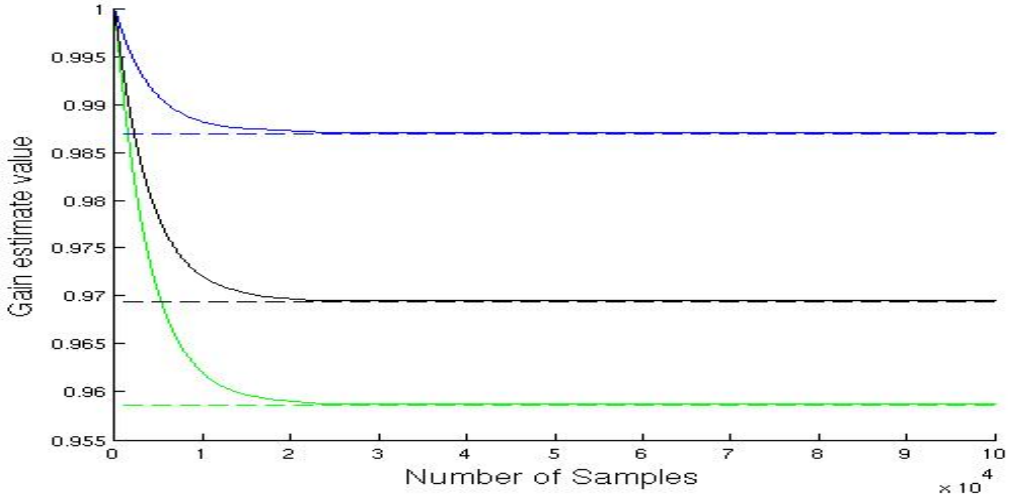

FIGURE 4.6: Convergence of Absolute value algorithm with notch filter for $f = 0.24$

Chapter 5

Gain Calibration by Oversampling Input Signal

A semi-blind more complicated calibration method is presented in Huang and Levy [2006], and further explored in Huang and Levy [2007]. If the input signal $x(t)$ is slightly oversampled, there will be some added redundancy to the set of sampled subchannel signals $y_i[m]$, $i \in 1..M$. This redundancy can be exploited in order to calibrate Gain mismatch, even though Huang and Levy [2006] and [Huang and Levy, 2007] use it mainly as a tool for calibrating the Timing offset.

5.1 Spectral Analysis of Sampled Signal

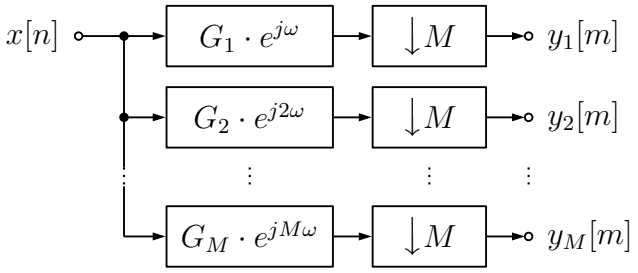

FIGURE 5.1: Filterbank equivalent of interleaved ADCs

A frequency analysis of the sampled signal is necessary in order to present the calibration method. If $X(\omega)$ is the DTFT of the ideally sampled signal $x(nT_s)$, the vector $\boldsymbol{X}(\omega)$ as given by Equation (5.1) consists of the M different aliases present when $x(nT_s)$ is downsampled by a factor M. Additionally, the vector $\boldsymbol{Y}(\omega)$ in Equation (5.2) consists of the DTFT of the set of M subchannel signals $y_i[m]$, $i \in 1..M$.

$$\boldsymbol{X}(\omega) = \begin{bmatrix} X(\frac{\omega}{M}) & X(\frac{\omega}{M} + \frac{2\pi}{M}) & \dots & X(\frac{\omega}{M} + (M-1)\frac{2\pi}{M}) \end{bmatrix}^T \tag{5.1}$$

$$\boldsymbol{Y}(\omega) = \begin{bmatrix} Y_1(\omega) & Y_2(\omega) & \dots & Y_M(\omega) \end{bmatrix}^T \tag{5.2}$$

Sampling with interleaved ADCs can be equated to filtering the discrete-time signal $x[n]$ through a filterbank of M allpass filters with the response $G_i \cdot e^{j(i-1)\omega}$, $i \in 1 \dots M$ followed by interpolation by a factor M. As such, the vector $\boldsymbol{Y}(\omega)$ can be given by $\boldsymbol{X}(\omega)$ as described by Equation (5.3) where the matrix $\boldsymbol{W}(\omega)$ is given by Equation (5.4).

$$\boldsymbol{Y}(\omega) = \frac{1}{M}\boldsymbol{W}(\omega) \cdot \boldsymbol{X}(\omega) \tag{5.3}$$

$$\boldsymbol{W}(\omega) = \begin{bmatrix} G_1 & G_1 & \dots & G_1 \\ G_2 e^{j\frac{\omega}{M}} & G_2 e^{j\frac{\omega+2\pi}{M}} & \dots & G_2 e^{j\frac{\omega+(M-1)2\pi}{M}} \\ \vdots & \vdots & \ddots & \vdots \\ G_M e^{j(M-1)\frac{\omega}{M}} & G_M e^{j(M-1)\frac{\omega+2\pi}{M}} & \dots & G_M e^{j(M-1)\frac{\omega+(M-1)2\pi}{M}} \end{bmatrix} \tag{5.4}$$

To conclude, each subchannel signal $y_i(n)$ is the sum of M components each representing a fraction of the signal spectrum $\frac{\pi}{M}$ wide. Since $\boldsymbol{X}(\omega)$ is unknown, it is not possible to calculate the Gain values.

5.2 Oversampling

Given an unknown input signal $x(t)$ with bandwidth $B = (1-\alpha)\frac{F_s}{2}$, the sampled signal $x(nT_s)$ will contain a band $|\omega| > (1-\alpha)\pi$ where spectral energy should be

zero. Assuming $\alpha < \frac{1}{M}$ and M is even, lowpass filtering each subchannel signal $y(n)$ with the ideal filter in Equation (5.5) will produce a signal with $M-1$ aliases.

$$H_{LP}(\omega) = \begin{cases} 1 & , |\omega| < \alpha \cdot M\pi \\ 0 & , |\omega| > \alpha \cdot M\pi \end{cases} \tag{5.5}$$

$$\boldsymbol{V}(\omega) = \begin{bmatrix} H_{LP}(\omega) & 0 & \dots & 0 \\ 0 & H_{LP}(\omega)e^{-j\frac{\omega}{M}} & \dots & 0 \\ \vdots & \vdots & \ddots & \vdots \\ 0 & 0 & \dots & H_{LP}(\omega)e^{-j\frac{(M-1)\omega}{M}} \end{bmatrix} \boldsymbol{Y}(\omega) \tag{5.6}$$

Because $\boldsymbol{V}(\omega)$ is given by Equation (5.6) and $H_{LP}(\omega)X(\frac{\omega}{M}+\pi) = 0$ when $X(\omega) = 0$, $|\omega| > (1-\alpha)\pi$, the vector $\boldsymbol{V}(\omega)$ can be given by Equation (5.7). $\boldsymbol{G}$ is the diagonal $M\,x\,M$ Gain matrix in Equation (5.8), $\boldsymbol{D}$ is the $M\,x\,(M-1)$ pangular delay matrix in Equation (5.9) and $\boldsymbol{X_{LP}}(\omega)$ is the vector of $(M-1)$ existing alias components in Equation (5.10).

$$\boldsymbol{V}(\omega) = \frac{1}{M}\,\boldsymbol{G}\,\boldsymbol{D}\,\boldsymbol{X_{LP}}(\omega) \tag{5.7}$$

$$\boldsymbol{G} = \begin{bmatrix} G_1 & \dots & 0 \\ \vdots & \ddots & \vdots \\ 0 & \dots & G_M \end{bmatrix} \tag{5.8}$$

$$\boldsymbol{D} = \begin{bmatrix} 1 & 1 & \dots & 1 \\ e^{j\frac{-M+2}{M}\pi} & e^{j\frac{-M+4}{M}\pi} & \dots & e^{j\frac{M-2}{M}\pi} \\ \vdots & \vdots & \ddots & \vdots \\ e^{j(M-1)\frac{-M+2}{M}\pi} & e^{j(M-1)\frac{-M+4}{M}\pi} & \dots & e^{j(M-1)\frac{M-2}{M}\pi} \end{bmatrix} \tag{5.9}$$

$$\boldsymbol{X_{LP}}(\omega) = \begin{bmatrix} H_{LP}(\omega)X(\frac{\omega}{M} + \frac{-M+2}{M}\pi) \\ H_{LP}(\omega)X(\frac{\omega}{M} + \frac{-M+4}{M}\pi) \\ \vdots \\ H_{LP}(\omega)X(\frac{\omega}{M} + \frac{M-2}{M}\pi) \end{bmatrix} \tag{5.10}$$

The advantage to $\boldsymbol{X_{LP}}(\omega)$ consisting of $(M-1)$ elements is there exists now a vector $\boldsymbol{c}(\boldsymbol{G})$ which fulfills the requirement $\boldsymbol{V}^T(\omega)\,\boldsymbol{c} = 0$. This is possible because $\boldsymbol{c}^T \cdot \boldsymbol{GD} \cdot \boldsymbol{1}$ can be formulated as a set of $(M-1)$ equations with $(M-1)$ unknown variables.

In *cite* solving this set of equations is a complicated procedure necessitating the use of Cramer's rule. However, when calculating the Gain mismatch the problem becomes much simpler, because every column in $\boldsymbol{D}$ except column $\frac{M}{2}$ will always contain the negative of any other value in the column interspersed by an odd number. Because of the absence of a column in $\boldsymbol{D}$ with the sequence $\begin{bmatrix}1 & e^{j\pi} & \dots & e^{j(M-1)\pi}\end{bmatrix}$ Equation (5.11) can be deemed valid.

$$\begin{bmatrix}1 & -1 & \dots & (-1)^{M-1}\end{bmatrix} \boldsymbol{D} = \begin{bmatrix}0 & 0 & \dots & 0\end{bmatrix} \tag{5.11}$$

Taking this into account, the vector $\boldsymbol{c}(\boldsymbol{G})$ can be any vector consistent with Equation (5.12), where k is a real constant with any value.

$$\boldsymbol{c}(\boldsymbol{G}) = k \begin{bmatrix} \frac{1}{G_1} \\ \frac{-1}{G_2} \\ \vdots \\ \frac{(-1)^{M-1}}{G_M} \end{bmatrix} \tag{5.12}$$

5.3 Calibration

By using Gain estimates to find an estimate of $\boldsymbol{c}(\boldsymbol{G})$ an error sequence can be generated for use in a LMS algorithm. $\hat{\boldsymbol{c}}(\hat{\boldsymbol{G}}[m])$ is given by Equation (5.13) where the optimal value of each Gain mismatch estimate is $opt(\hat{G}_i[m]) = \frac{G_1}{G_i}, \quad i \in 2..M$.

$$\hat{\boldsymbol{c}}(\hat{\boldsymbol{G}}[m]) = \begin{bmatrix}1 & \hat{G}_2[m] & \dots & \hat{G}_M[m]\end{bmatrix}^T \tag{5.13}$$

$$\epsilon[m] = \hat{\boldsymbol{c}}(\hat{\boldsymbol{G}}[m])^T\, \boldsymbol{V}[m] \tag{5.14}$$

Using the error signal in Equation (5.14) the Gain mismatch estimates $\hat{G}_i[m], \quad i \in 2..M$ can be found by updating estimates according to the algorithm in Equation (5.15), where the step size μ_G is governs how quickly the Gain mismatch estimates converge with the actual Gain mismatch.

$$\hat{G}_i[m+1] = \hat{G}_i[m] + (-1)^i \cdot v_i[m] \cdot \epsilon[m] \cdot \mu_G \tag{5.15}$$

An implementation of the system is shown in Figure 5.2. The filters which make up the filter bank $H_{LP}(\omega)e^{-j\frac{2i\pi}{M}}, \quad i \in 0..(M-1)$ can be implemented using fractional delay FIR filters, which are explained in [Laakso et al., 1996].

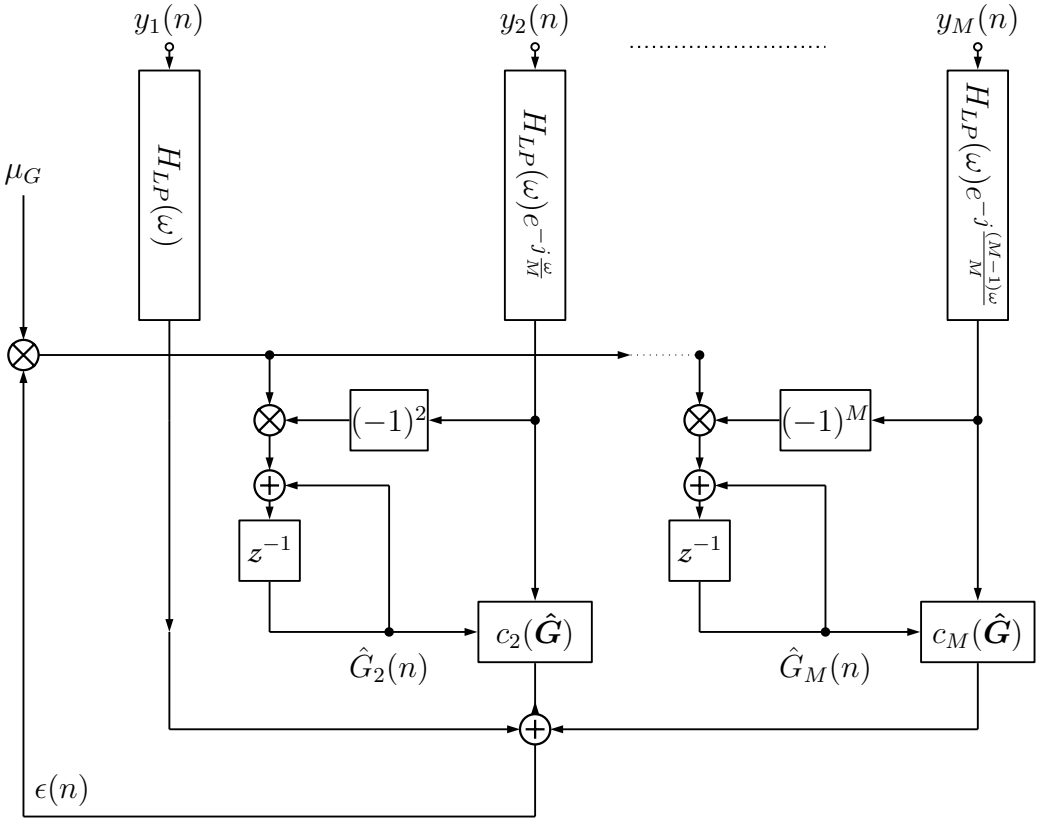

FIGURE 5.2: Calibration system based on a bandlimited input signal

5.4 Convergence Analysis

A prerequisite for the calibration system in Figure 5.2 is the presence of signal power in the subchannel signals $y_i[m]$, $i \in [1, M]$ in the band $0 < f < M \cdot \alpha$. Otherwise, the elements in $\boldsymbol{V}(\omega)$ will not contain spectral power at all, resulting in a absence of information that can be used to estimate Gain mismatches.

The frequency bands of the oversampled input signal which are not blocked by the filters H_{LP} once it has been downsampled by a factor M, are given by Equation (5.16).

$$f \in \begin{cases} |f| < \alpha \\ \frac{2}{M} - \alpha < |f| < \frac{2}{M} + \alpha \\ \quad \vdots \\ \frac{M-2}{M} - \alpha < |f| < \frac{M-2}{M} + \alpha \end{cases} \tag{5.16}$$

The frequency band $1-\alpha < f < 1$ is reserved for signal images resulting from Gain mismatch, the presence of which is the basis of estimating the Gain mismatches. Once $M > 2$ however, there are instances where certain Gain mismatches may avoid detection.

If the spectral power of $x[n]$ is contained within only one of the bands given in Equation (5.16), Gain mismatches of a certain form can cause images of the signal to manifest in a number of the other bands in Equation (5.16) but not in the band $1 - \alpha < f < 14$. The consequence such an input signal is that different subsets of the M subchannels can be calibrated independently of each other.

To take an example; if $M = 4$ and $x(t)$ is a sine wave with $\frac{1}{2} - \alpha < 2\frac{F_x}{F_s} < \frac{1}{2} + \alpha$, Gain mismatch can be expected to cause images of $x[n]$ with $f = 2\frac{F_x}{F_s} + \frac{i}{2}$, $i \in [1, 3]$. However, if Gain mismatch is only partially calibrated so $G_1 = G_3 \cdot \hat{G}_3[m]$ and $G_2 \cdot \hat{G}_2[m] = G_4 \cdot \hat{G}_4[m]$, there will only be a signal image for $f = 2\frac{F_x}{F_s} + 1$. As a result, there are now two subsets of Gain estimates which are calibrated within each subset, but not between the subsets.

To conclude, in order to guarantee that all Gain estimates are matched with the same reference value, the input signal $x[n]$ should have components within all the frequency bands described by Equation (5.16).

5.5 Quantization

Fixed point representation of the various signal values is done in a similar fashion to Chapters 3 and 4. The signals $y_i[m]$ and $\epsilon[m]$ are represented using b_y bits, while the estimates $\hat{G}_i[m]$ should be represented using a larger number of bits. The order of operations in Figure 5.2 will have to be modified somewhat, so the product of multiplying by the step factor μ_G is represented in higher precision than b_y bits allow.

Assuming truncation does not occur within the fractional delay filters themselves, white uncorrelated uniformly distributed noise with PDF $P = \mathcal{U}(-\frac{\Delta_q}{2}, \frac{\Delta_q}{2})$ will be added to the signals after filtering, and after multiplying by the vector $\hat{\boldsymbol{c}}(\hat{\boldsymbol{G}}[m])$. All these are approximately added together, since the elements in $\hat{\boldsymbol{c}}(\hat{\boldsymbol{G}}[m])$ re relatively close to 1. As a consequence, the error signal used for calibration will be distorted by a noise signal $\nu_\epsilon[m]$ with variance given by Equation (5.17).

$$Var(\nu_\epsilon[m]) \approx (2M-1)\frac{\Delta_q^2}{12} \tag{5.17}$$

Seeing as $\epsilon[m]$ forms the basis for all the Gain estimates, it seems prudent to ensure that $\nu_\epsilon[m]$ has minimal effect on the Gain estimates. If the quantization errors added after filtering is temporarily assumed to not be altered by multiplying by the vector $\hat{\boldsymbol{c}}(\hat{\boldsymbol{G}}[m])$, then the effect of quantization error on the Gain estimate can be compared to the signal $\nu_G[m]$ in Equation (5.18).

$$\nu_G[m] = \nu_\epsilon[m] * h_G[m] \tag{5.18}$$

$h_G[m]$ in Equation (5.18) is the IIR filter given by Equation (5.19).

$$h_G[m] = \mu_G \cdot (1 - \mu_G)^m \tag{5.19}$$

The variance of ν_G will in this case be given as

$$Var(\nu_G[m]) = (2M - 1)\frac{\mu_G \Delta_q^2}{24} \tag{5.20}$$

once the filter is in steady state. This gives an indication of what value μ_G must have for $\nu_G[m]$ to be eclipsed by the quantization error which occurs when the estimates $\hat{G}_i[m]$ are truncated to b_y bits. By setting the condition $Var(\nu_G[m]) < \frac{\Delta_q^2}{12}$, the upper limit for the step size μ_G is found to be

$$\mu_G < \frac{2}{2M - 1} \approx \frac{1}{M} \tag{5.21}$$

5.6 Numerical Simulations

The calibration system is tested multiple times using randomly generated Gain values. Offset standard deviation is set to $\sigma_G = 0.05V$, and simulations are conducted assuming $M = 4$ interleaved ADCs. Estimator convergence is tested using both AWGN and sinusoidal signals as input, and AWGN input is used to find more extensive data concerning the Mean Square Error(MSE) of the estimator given sample number m.

The approximate MSE sequences are considered in relation to the minimum obtainable MSE according to theory $E(J_{min}[m]) = 2 \cdot \frac{\Delta_q^2}{12} = E((\nu_{i1}[m] + \nu_{i2}[m])^2)$. Multiple different sample resolutions are used.

The calibration system is implemented using $\alpha = \frac{1}{2M}$ denoting the unused frequency band. The fractional filters are chosen to be 48-tap filters set to have a transition band $0.3 < f < 0.5$, so the stopband covers all the entire band where all aliases are present. The fractional delay filters are found using FIR filters from

the *firls* function in MATLAB, and converting them to fractional delay filters as described in Laakso et al. [1996] using no window function.

The system is also tested using input signals with components in only one of the necessary frequency bands described by Equation (5.16) in order to illustrate the effect this will have on the calibration system.

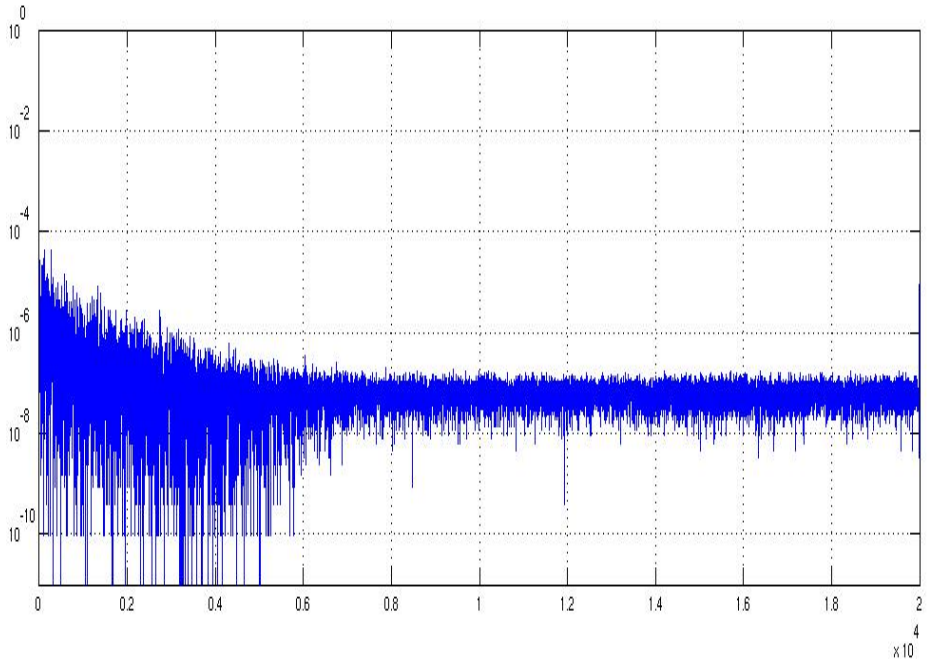

FIGURE 5.3: Average error sequence $\epsilon[m]$ for a AWGN input signal $\sigma_x = 0.3$

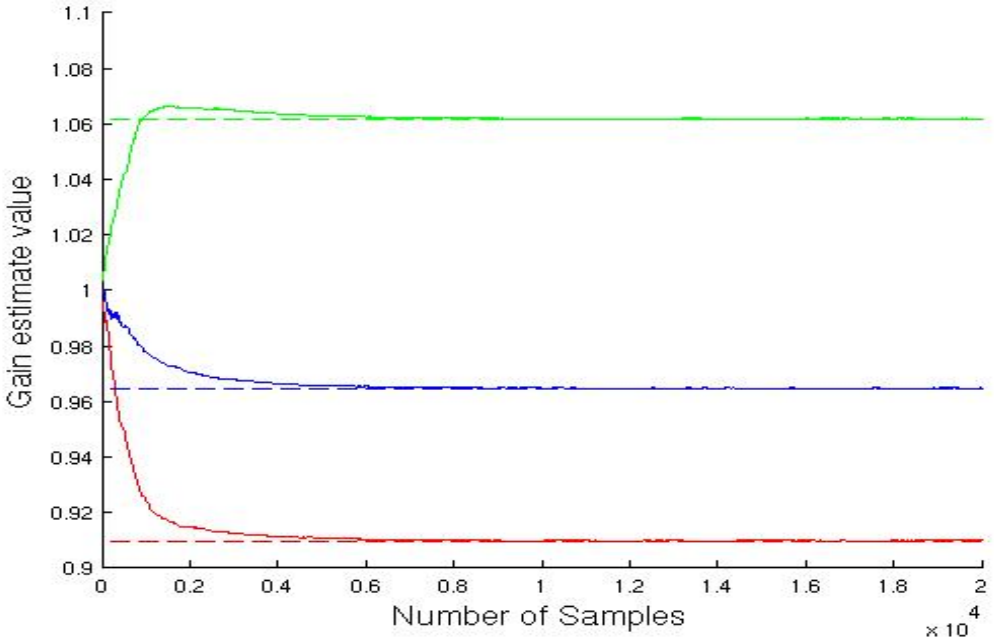

FIGURE 5.4: Convergence of Gain estimates for AWGN input signal $\sigma_x = 0.3$

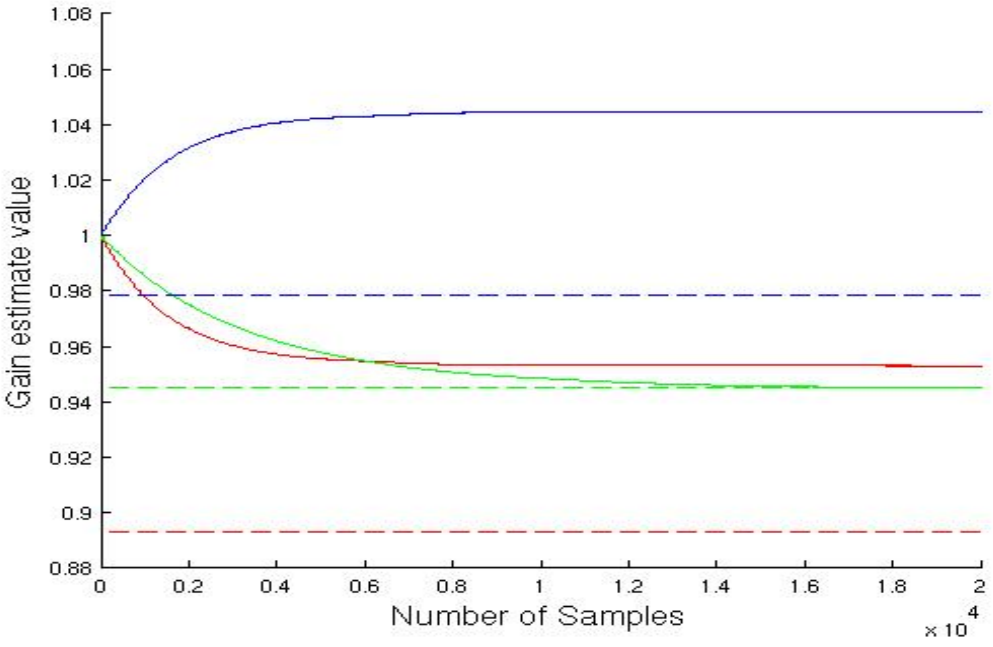

FIGURE 5.5: Convergence of Gain estimates for single sine component $f = 0.24$, $\sigma_x^2 = 0.01$.

5.7 Discussion

There is one notable difference between the calibration system in Figure 5.2 and the ones presented in Chapter 3 and 4. The previous calibration systems rely on generating a error sequence which has an average of zero once Gain mismatch has been correctly estimated. In contrast, this system generates a error sequence consequently equal to zero if the Gain estimates are correct.

Ideally, the only distortion present to cause deviation in the error sequence would be caused by quantization. However, the fractional delay filters implemented will not be ideal and deviations in passband ripple as well as nonzero stopband attenuation will each add distortion to the error sequence.

The level of deviation in the error sequence will still be very small, permitting a step size μ_G many orders of magnitude larger than in previous calibration systems. As a result, the convergence time of this system will in theory be significantly reduced.

As seen in Figure 5.5, the Gain estimates seem to be calibrated halfway. $\hat{G}_3[m]$ reaches the correct value, while $\hat{G}_2[m]$ and $\hat{G}_4[m]$ reach a correct distance between each other, but the pair of estimates are skewed. To conclude, complete calibration will require signal components in all the frequency bands used for calibration.

Chapter 6

Concluding Remarks

6.1 Conclusion

A selection of existing Gain and Offset calibration algorithms have been studied. These consist of a simple averaging algorithm for Offset calibration, and three separate Gain calibration algorithms. One Gain calibration algorithm utilizes a training signal, and a potentially beneficial modification incorporating prior knowledge has been suggested. Another algorithm which compares the average power of two ADC outputs has been studied using multiple possible approaches. A third algorithm is based on adding redundancy through oversampling the input signal.

The received signal is assumed to be sampled using fixed-point precision, using any of a variety of relevant sampling resolutions. Testing of the calibration systems is done numerically using a variety of input signals consisting of white Gaussian noise and sinusoidal sequences.

The Offset calibration method is found to perform consistently for all chopped input signals. Utilizing prior knowledge is shown to improve it's rate of convergence considerably.

The Gain calibration method utilizing a training sequence is shown to have a consistent convergence rate regardless of input, but is found to be relatively inefficient as it does not make use of the input signal in any way. Incorporating prior knowledge estimation did improve the rate of convergence to some extent.

Comparing subchannel power, despite being inefficient for low-power input signals can be said to be the most convenient approach studied. It places no restrictions on the input signal, and though certain input signals components can cause instability, the absence of these components can be guaranteed using simple low order filters. Applying this calibration method to an arbitrary number of interleaved ADCs is relatively simple, and will not increase the system's degree of complexity.

The system also permits various changes to be made, which can increase performance with a few added arithmetic operations. Most interestingly, using a relatively simple IIR notch filter, rather than the FIR filter initially suggested, results in a considerably wider frequency band where useful signal components are used to their full potential. Additionally, by comparing the average absolute value rather than signal power the convergence rate is less affected by input signal power.

The added redundancy from oversampling the signal when combined with signals with the necessary spectral content is proven to be incredibly efficient. It has a convergence rate many orders of magnitude faster than the two other algorithms. Filter design is crucial for this algorithm however, and a stable output in all circumstances may require higher order FIR filters than what is preferable. While this calibration system can be used to calibrate Gain mismatch for any even number of interleaved ADCs, reliable estimation is rather dependent on the input signal fulfilling a number of requirements increasing with the number of ADCs to be calibrated.

All of the calibration systems have been analyzed with the goal of finding close to ideal tuning. The theoretical tuning has been tested extensively using a number of different sampling resolutions. The tuned calibration systems are shown to achieve

distortion levels relatively close to the minimal distortion levels theoretically obtainable, while still maintaining a reasonable tracking speed.

6.2 Further Work

The most important subject for further investigation should be how the calibration system will react to real-world data, not just mathematically generated signals. The simulations conducted during the course of this thesis are all generated digitally, based on theoretical ADC properties. Whether or not the algorithms will work sufficiently with received samples from a set of real ADCs remains to be seen.

One property of such digital calibration systems which has not been measured is the number of logical operations required for each iteration of the adaptive systems. Since the methods debated are intended for use in small electronic components operating at very high clock frequencies, minimizing the amount of logical operations will be of great concern.

Bibliography

C. Vogel. The impact of combined channel mismatch effects in time-interleaved adcs. *Instrumentation and Measurement, IEEE Transactions on*, 54(1):415–427, 2005.

D. Fu, K.C. Dyer, S.H. Lewis, and P.J. Hurst. A digital background calibration technique for time-interleaved analog-to-digital converters. *Solid-State Circuits, IEEE Journal of*, 33(12):1904–1911, 1998.

S.M. Jamal, D. Fu, N.C.-J. Chang, P.J. Hurst, and S.H. Lewis. A 10-b 120-msample/s time-interleaved analog-to-digital converter with digital background calibration. *Solid-State Circuits, IEEE Journal of*, 37(12):1618–1627, 2002.

S. Huang and B.C. Levy. Adaptive blind calibration of timing offset and gain mismatch for two-channel time-interleaved adcs. *Circuits and Systems I: Regular Papers, IEEE Transactions on*, 53(6):1278–1288, 2006.

S. Huang and B.C. Levy. Blind calibration of timing offsets for four-channel time-interleaved adcs. *Circuits and Systems I: Regular Papers, IEEE Transactions on*, 54(4):863–876, April 2007.

S. M. Kay. *Fundamentals of Statistical Signal Processing. Vol 1: Estimation Theory*. Prentice-Hall Inc., 1993.

M. Salehi J. G. Proakis. *Digital Communications*. McGraw Hill, 2008.

T.I. Laakso, V. Valimaki, M. Karjalainen, and U.K. Laine. Splitting the unit delay [fir/all pass filters design]. *Signal Processing Magazine, IEEE*, 13(1):30–60, 1996.

Study of variable step size

.1 Offset Calibration

In the case where the intent is to estimate Offset in a noisy signal, the basic calibration algorithm is given as

$$\hat{A}(n+1) = y(n) \cdot \mu_A + (1 - \mu_A) \cdot \hat{A}(n). \tag{1}$$

$$\mu_A(n) = \frac{\beta}{\alpha + \beta n} \tag{2}$$

Substituting the constant step size μ_A in Equation (1) with a variable step size $\mu_A(n)$ given by Equation (2) presents a Offset estimate given by Equation (3a). By expanding the series, the estimate in Equation (3g) presents itself, which is identical to that of a MAP estimator.

$$\hat{A}(n+1) = y(n) \cdot \frac{\beta}{\alpha+\beta n} + \big(1 - \frac{\beta}{\alpha+\beta n}\big) \cdot \hat{A}(n) \tag{3a}$$

$$= y(n) \cdot \frac{\beta}{\alpha+\beta n} + y(n-1) \cdot \frac{\alpha+\beta(n-1)}{\alpha+\beta n} \cdot \frac{\beta}{\alpha+\beta(n-1)} + \frac{\alpha+\beta(n-1)}{\alpha+\beta n} \cdot \frac{\alpha+\beta(n-2)}{\alpha+\beta(n-1)} \cdot \hat{A}(n-1) \tag{3b}$$

$$= \sum_{k=1}^{n} \frac{y(k) \cdot \beta}{\alpha+\beta k} \prod_{i=k+1}^{n} \frac{\alpha+\beta(i-1)}{\alpha+\beta i} + \prod_{i=1}^{n} \frac{\alpha+\beta(i-1)}{\alpha+\beta i} \cdot \hat{A}(0) \tag{3c}$$

$$\prod_{i=k}^{n} \frac{\alpha+\beta(i-1)}{\alpha+\beta i} = \frac{\alpha+\beta(n-1)}{\alpha+\beta n} \frac{\alpha+\beta(n-2)}{\alpha+\beta(n-1)} \cdots \frac{\alpha+\beta(k-1)}{\alpha+\beta(k)} \tag{3d}$$

$$= \frac{\alpha+\beta(k-1)}{\alpha+\beta n} \tag{3e}$$

$$\hat{A}(n+1) = \sum_{k=1}^{n} \frac{y(k) \cdot \beta}{\alpha+\beta k} \cdot \frac{\alpha+\beta k}{\alpha+\beta n} + \frac{\alpha}{\alpha+\beta n} \cdot \hat{A}(0) \tag{3f}$$

$$= \sum_{k=1}^{n} y(k) \cdot \frac{\beta}{\alpha+\beta n} + \hat{A}(0) \cdot \frac{\alpha}{\alpha+\beta n} \tag{3g}$$

By replacing α and β in Equation (**??**) with σ_y^2 and σ_A^2 respectively, the calibration algorithm will produce the MAP estimate of the Offset A. The only problem is that the signal energy σ_y^2 is unknown.

If the estimator in Equation (2.9) is assigned a upper bound for σ_y^2, it will not always produce the most likely estimate. On the other hand, it will be stable and will still converge with the value A a lot faster than Equation (2.3).

.2 Gain Calibration

Equations (3.6) and (3.7) indicate a gradually decreasing step size may be beneficial for this algorithm. As in Chapter 2, we suggest the use of a variable step size scaled by a factor k^{-2}, given by Equation (4). By using Equation (3.4), the expected value can be found as given by Equation (5). This equation can not be simplified to the form of a recognizable estimator, but the deviation from a desired output can still be found for specific values of α and β.

$$\mu_G(n) = \frac{1}{k^2}\frac{\alpha}{\alpha+\beta n} \tag{4}$$

$$E(\hat{G}(n)) = \sum_{i=1}^{n}\left(\frac{\beta}{\alpha+\beta n}\prod_{j=i+1}^{n}\left(\frac{\alpha+\beta(j-G_AG_D)}{\alpha+\beta j}\right)\right) + \hat{G}(0)\prod_{i=1}^{n}\left(\frac{\alpha+\beta(i-G_AG_D)}{\alpha+\beta i}\right) \tag{5}$$

Assuming the Gain factors have a Gaussian PDF with variance $Var(G) = \sigma_G^2$, a MAP Estimator for the Gain factor G_AG_D can be found by using the error signal given by Equation (3.2). Given a chopped input signal, the average of the error signal $\bar{\epsilon}(n)$ can be assumed to have a Gaussian probability distribution described by Equation (6).

$$P(\bar{\epsilon}(n)|G_DG_A) \sim \mathcal{N}(G_DG_A - 1, \frac{\sigma_x^2}{\sqrt{n}}) \tag{6}$$

$$Var(G_AG_D) = 2\sigma_G^2 + \sigma_G^4 \tag{7}$$

Bayes' Theorem and Equations (6) and (7) combined produce a MAP estimator for the gain factor G_DG_A given by equation (8)

$$max(P((G_AG_D)|\bar{\epsilon}(n))) = \frac{\bar{\epsilon}(n)\cdot n}{\frac{\sigma_x^2}{2\sigma_G^2+\sigma_G^4} + n\cdot k^2} + 1 \tag{8}$$

As in Chapter 2, $\sigma_x^2 = 0.5$ is a reasonable worst-case value which will still produce an acceptable estimator. It is of interest to compare Equation (8) to Equation (5) with variable step factor given by Equation (9).

$$\mu_G(n) = \frac{1}{\frac{max(\sigma_x^2)}{2\sigma_G^2+\sigma_G^4} + k^2\cdot n} \tag{9}$$

Assuming $\sigma_G = 0.05$ [1] for both G_A and G_D, the standard deviation of the total gain factor $G_A G_D$ is equal to $\sigma_{prod} = \sqrt{2\sigma_G^2 + \sigma^4} \approx 0.071$. Figure 1 shows the output of Equations (5) and (8) for extreme values of gain mismatch. Figure 2 shows the maximum deviation of the two functions given the total Gain factor $G_A G_D$. Using Figure 2 and the Gaussian distribution function, we find the probability of a deviation larger than 0.01 to be approximately $5.27 \cdot 10^{-5}$.

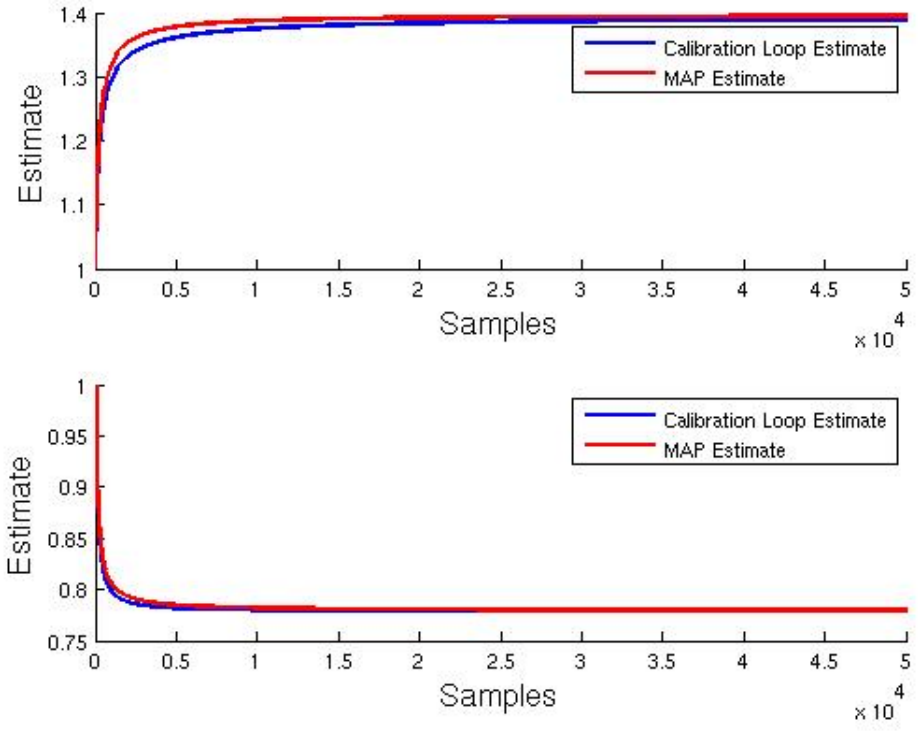

FIGURE 1: Convergence of both estimates with $G_A G_D = 1 \pm 4 \cdot \sigma_{prod}$

To summarize, it is safe to assume that for the overwhelming majority of possible Gain factor values, using the variable step factor in Equation (9) will produce a reliable estimate of $G_D G_A$.

[1] Specified by project co-supervisor

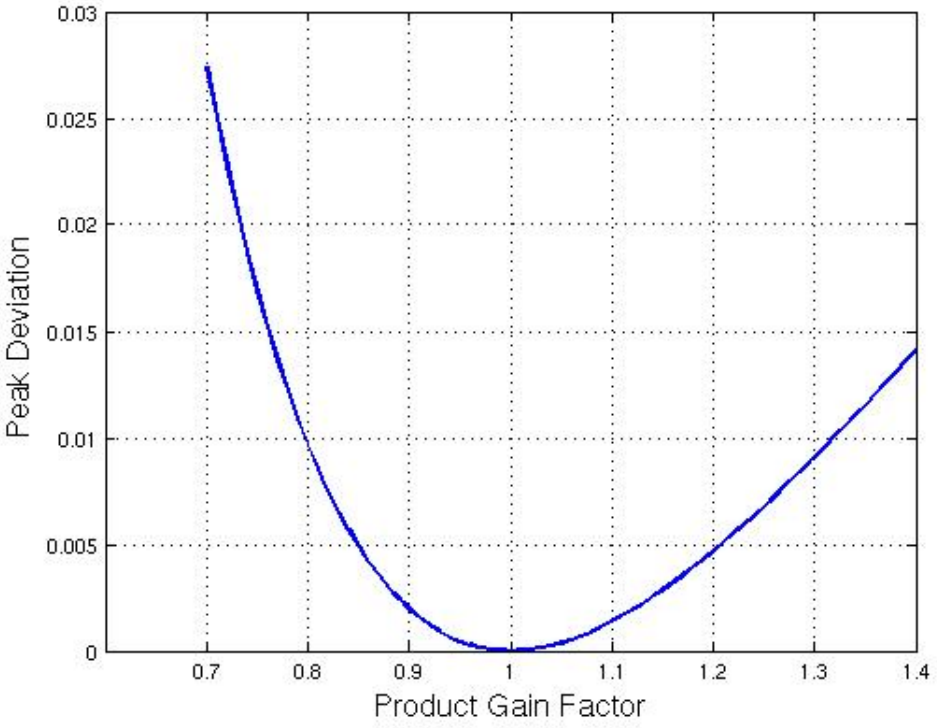

FIGURE 2: Peak deviation between the estimates